Exploring the scope of BTA based organocatalysts in water

Neumann, L.N.

Award date:
2015

Exploring the scope of BTA based organocatalysts in water

Graduation report of

L.N. Neumann

Molecular Engineering Master Program

Eindhoven University of Technology

Exploring the scope of BTA based organocatalysts in water

Graduation Report of

Laura Noëlle Neumann

Supervisors:
Ir. C. M. A. Leenders
Dr. M. Baker
Dr. Ir. A. R. A. Palmans

Supervising Professor:
Prof. Dr. E. W. Meijer

Advising Committee:
Dr. Ir. J. P. A. Heuts

Eindhoven, September 2014

Laboratory of Macromolecular and Organic Chemistry
Faculty of Chemical Engineering and Chemistry
Eindhoven University of Technology

Summary

Enzymes are considered to be the most efficient catalysts known in terms of activity and selectivity. These excellent catalytic properties arise due to the a very specific three-dimensional structure of enzymes in which the catalyst is shielded from the outside environment. Scientists developed various enzyme mimics based on this principle in order to design highly selective and active catalysis.

In this project, we designed an enzyme mimic based on water soluble benzene-1,3,5-tricarboxamides (BTAs) functionalized with a catalytic *L*-proline moiety. In water, these BTAs self-assemble into well-defined supramolecular stacks. Incorporation of the *L*-proline moieties into the hydrophobic core of these stacks yielded a highly active and selective catalyst. The possibility to tune the local *L*-proline density in the stacks, allows for control over this well-defined system.

Two different molecular designs were explored; one symmetric BTA that contains three *L*-proline moieties on the periphery (compound **1**), and one asymmetric BTA that contains a single *L*-proline functionality in the hydrophobic environment of the BTA (compound **2**). The successful synthesis and characterization of these two BTAs is described in chapter 2.

The self-assembly of the functionalized BTAs was studied in detail using various techniques including UV-Vis spectroscopy, circulair dichorism (CD) spectroscopy, dynamic light scattering (DLS), small-angle X-ray scattering (SAXS), and cryogenic transmission electron microscopy (cryo-TEM). A combination of the results suggests self-assembly of **1** into spherical objects whereas **2** was shown to self-assemble into one-dimensional fibers.

The catalytic activity of the system was explored, by using the model aldol reaction between 4-nitrobenzaldehyde and cyclohexanone. While most organocatalytic systems in water operate at catalyst concentrations above 5 mol%, **1** was found to show quantitative conversion and moderate selectivity (diastomeric excess = 64%, enantiomeric excess = 65%) at a catalyst loading of 3 mol%.

BTA **2** was shown to be an even more active and selective catalyst, since quantitative conversion and excellent selectivities up to *de* = 96% and *ee* = 97% were obtained at a catalyst loading as low as 1 mol%. Furthermore, the catalytic behavior was shown to be very reproducible, since six different samples showed a consistent conversion of 92 ± 8%, a *de* = 92 ± 3%, and *ee* = 97 ± 1%. Besides that, **2** is still active at a catalyst loading of 0.2 mol%, which is among the lowest catalyst loadings reported in literature.

Table of contents

Chapter 1 Introduction

"…where nature finishes producing its species, there man begins with natural things to make, with the aid of this nature, an infinite number of species…"[1]

Leonardo da Vinci

The beauty of natural systems has always been a great source of inspiration for humankind. For millennia, people have tried to mimic natural systems in order to produce novel materials and technologies.

For example, the wish to fly has always been cherished by humankind and extensive effort has been put into the development of equipment to come closer to achieving bird flight. Leonardo da Vinci built his well-known rudimentary flapping wing model in 1490 and the effort to decipher bird flight has continued ever since. A very recent development constitutes the launch of SmartBird (Figure 1.1), an ornithopter modeled on the herring gull able to take off, fly and land by itself.[2]

Figure 1.1: Festno's SmartBird[2]

The development of equipment allowing humans to experience bird flight is an example of efforts to mimic the complexity of macroscopic natural systems. However, also at the microscopic level, highly optimized systems can be observed in nature, which are usually incredibly complex, but sometimes elegantly simple. The ability of enzymes to perform catalysis with excellent efficiency and selectivity is an example of Natures' ability to form sophisticated structures at a microscopic level. The excellent catalytic properties of enzymes arise due to the formation of a specific three-dimensional structure by folding of the primary structure into a highly organized secondary and tertiary structure by non-covalent supramolecular interactions (Figure 1.2).

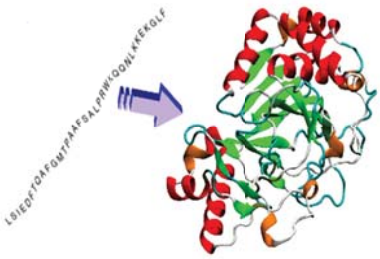

Figure 1.2: Folding of the primary structure of an enzyme into its active conformation.[3]

1.1. Supramolecular chemistry

Nature ubiquitously uses supramolecular interactions to create structures with extraordinary complexity. However, it took until the early 19th century before humankind started to explore and utilize supramolecular systems. Jean-Marie Lehn, who won the Nobel Prize for his work in this area in 1987, defined supramolecular chemistry as the chemistry of molecular assemblies and of the intermolecular bond.[4] The pioneering work done by Pedersen, Cram and Lehn covered the development of macrocyclic ligands able to selectively bind metal cations, using non-covalent ion-dipole interactions. Whereas this host-guest chemistry was the main area of research in the early years, currently the scope of supramolecular chemistry has been expanded to molecular devices and machines, molecular recognition and so-called 'self-processes' including self-assembly and self-organization, making supramolecular chemistry a highly interdisciplinary field.[5]

Various supramolecular interactions are used to create highly ordered structures, including ion-ion and ion-dipole interactions, hydrogen bonding, and the hydrophobic effect. The self-assembly of self-organizing monomers is based on (a combination of) these different non-covalent interactions. Various self-assembling motives have emerged, including phorphyrins,[6] 2-ureido-4-pyrimidinones,[7] and benzene-1,3,5-tricarboxamides.[8]

1.1.1. Benzene-1,3,5-tricarboxamides (BTAs)

Benzene-1,3,5-tricarboxamides (BTAs) consist of a benzene core with three amides connected at the 1, 3 and 5 positions (Figure 1.3). After they were described for the first time by Curtius in 1915, their simple structure and wide accessibility yielded a vast amount of research in both this group[9–11] and elsewhere[12,13] to elucidate the self-assembly behavior and develop new applications. Consequently, a large variety of applications of BTAs emerged in fields ranging from nanotechnology to polymer processing and biomedical applications. BTAs have been used in, for example, liquid crystals, organogels, hydrogels, MRI contrast reagents, and microcapsules for drug delivery.[8]

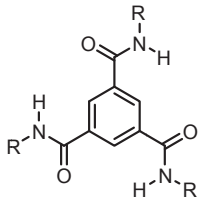

Figure 1.3: General chemical structure of a BTA.

BTAs bearing alkyl side-chains self-assemble in both the solid state and dilute, apolar organic solutions by means of strong, threefold intermolecular hydrogen bonding into well-defined, helical, one-dimensional columnar aggregates as shown in Figure 1.4.[14] Upon introduction of a stereogenic center into the alkyl side chain, a strong Cotton effect arises due to the preference to form either M- or P-helical stacks.[9,15] Formation of helical BTA aggregates occurs by the means of a cooperative mechanism starting with a nucleation phase followed by a more favorable elongation phase.[9]

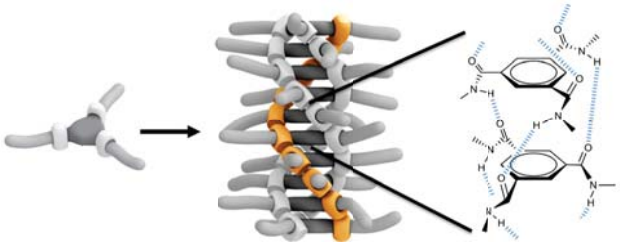

Figure 1.4: Schematic representation of benzene-1,3,5-tricarboxamide self-assembly into helical one-dimensional aggregates stabilized by threefold intermolecular H-bonding.[8]

The applications of BTAs bearing alkyl side chains are limited to apolar organic solvents. No stacks are formed in polar solvents like methanol or chloroform, since the BTAs are in the molecularly dissolved state.[16,17] Moreover, the design of the BTAs is not suitable for applications in water-based systems. However, having widespread applications in mind, it is very desirable to exchange organic solvents for water, as water is the most ubiquitous used solvent outside the lab. Moreover, water is a very cheap, abundant and non-toxic solvent.

In order to allow for self-assembly of BTAs in water, the molecular design needs to be altered. A convenient design of a water soluble BTA developed recently in our group consists of the BTA core bearing aliphatic chains to shield the central hydrogen bonding unit from the surrounding water, and hydrophilic ethylene glycol motifs on the periphery, to ensure solubility (Figure 1.5 A).[17] The stacking of these BTA is driven by hydrogen bonding and the hydrophobic effect, and was confirmed by UV-Vis absorption, circular dichroism (CD) spectroscopy and cryogenic transmission electron microscopy (cryo-TEM).

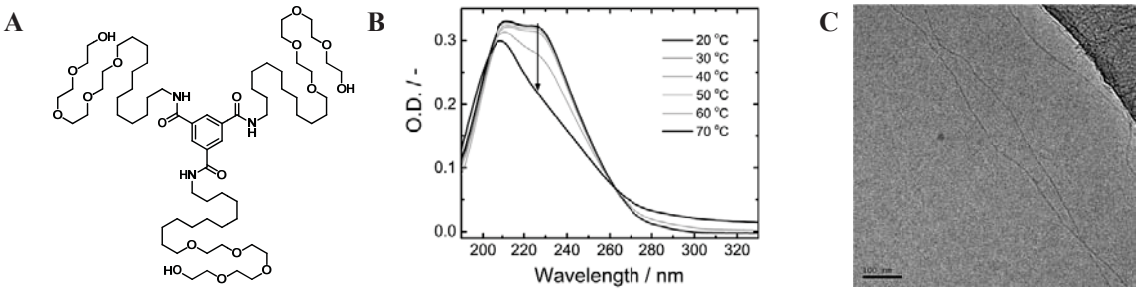

Figure 1.5: (A) Molecular structure of a water soluble BTA. (B) UV-Vis absorption of 1 (c = 1 x 10^{-5} M) in water, as a function of temperature (the arrow indicates the trend upon heating). (C) Cryo-TEM image of A in water, showing long very narrow fibrillar aggregates.[17]

In dilute aqueous solutions, the rationally designed water soluble BTA (Figure 1.5 A) shows a UV spectrum with two distinct absorption bands at 211 nm and 226 nm (Figure 1.5 B) indicative for the aggregated state. At elevated temperatures, however, only a single band at 209 nm is observed corresponding to aggregate disruption. Visualization by cryo-TEM shows the presence of long thin fibers with a high aspect ratio (Figure 1.5 C). This observation proves self-assembly of this water soluble BTA into one-dimensional supramolecular stacks in water.

Intrigued by the possibilities of the water soluble BTA, Albertazzi *et al.* developed a system to gain spatiotemporal control over functionalized monomers inside a supramolecular BTA-based polymer. For the development of this system, Albertazzi and coworkers took advantage of both the coassembly of dye-functionalized BTAs with non-functionalized BTAs, and the reversible interactions between monomers that result in a dynamic BTA stack where monomers are constantly being exchanged within the bulk fiber.[8,18] Introduction of a trigger that only has affinity for the functionalized monomers, resulted in a rearrangement of the monomer distribution along the polymer and reversible clustering of the functionalized monomers (Figure 1.6).[19]

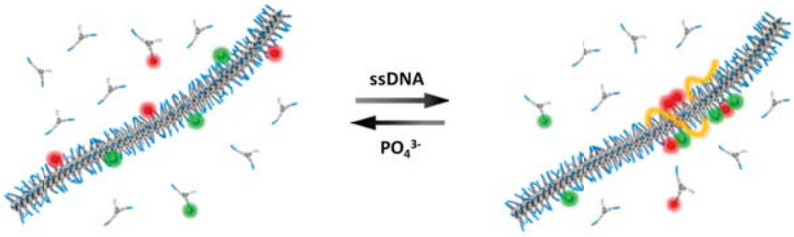

Figure 1.6: Coassembling unfunctionalized BTAs with functionalized BTA derivatives yields a supramolecular polymer (left). ssDNA is able to bind and recruit multiple functionalized monomers (right) thereby creating clustering along the supramolecular polymer.[19]

The development of water soluble BTAs and the ability to gain control over the monomer distribution within a supramolecular fiber gives rise to very intuiting potential applications of BTA scaffolds in enzyme mimics. Also in recent literature, responsive systems comparable to the system of Albertazzi *et al.* are reported. For example, Zhang and coworkers reported the self-assembly of

chemically sensitive gels caused by noncovalent interactions and subsequent disassembly in response to external stimuli.[20] More recently, also multi-controlled drugs release behavior became part of the chemists' toolbox.[21] The new developments in this field represent the next step towards the design of dynamic multi-responsive systems mimicking the complexity and functionality of natural systems.

1.2. *L*-Proline in organocatalytic systems

The field of asymmetric catalysis dates back to 1912 when Bredig reported a modestly enantioselective alkaloid-catalyzed cyanohydrin synthesis. Currently, the field of efficient asymmetric catalysis is flourishing due to the broad utility of synthetic chiral molecules in single-enantiomer pharmaceuticals, in electronic and optical devices, and as probes of biological function, among others.[22] Asymmetric catalysis was traditionally based on biocatalysis and metal catalysis. However, in the past two decades, organocatalysis developed as its own promising field.[22,23]

Proline was the first organocatalysts to be described[24] and due to its good catalytic properties combined with its easy availability and low costs, it is still one of the most investigated organocatalysts. Proline was found to catalyze a number of important C-C bond forming reactions; the most important and most studied one being the aldol reaction, where two carbonyl partners are united yielding ß-hydroxyketones with up to two new stereo centers (Scheme 1.1).[25] Other proline catalyzed reactions include Michael additions, Mannich reactions, Robinson ring annulation, and a range of other cycloaddition reactions.[26]

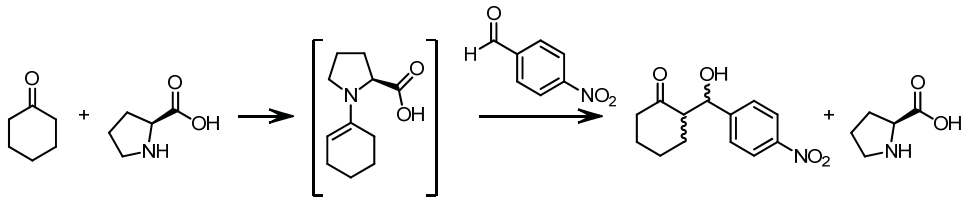

Scheme 1.1: The aldol reaction between cyclohexanone and 4-nitrobenzaldehyde catalyzed by *L*-proline.

The extensive use of *L*-proline as organocatalyst started in 2000 when List *et al.* published a paper on the use of this catalyst for a variety of aldol reactions.[27] Whereas for this study unmodified *L*-proline in DMSO at high catalyst loadings (30 mol%) was used, the years thereafter a lot of effort was put in modification of the *L*-proline to improve its catalytic properties to expand the substrate scope,[29] to enable low-loading organocatalysis,[30] and to allow for the scale-up of the process.[31] Furthermore, the addition of additives to improve the yield and selectivity,[28] the addition of water to accelerate the reaction[32,33] and, ultimately, the development of water compatible *L*-proline derivatives have been subjected to intensive research.[34–38]

1.2.1. *L*-Proline in water based organocatalytic systems

Generally, the use of water as a reaction solvent is not practical. Water often inhibits catalyst activity and frequently alters enantioselectivity by interruption of ionic interactions and hydrogen bonds which are critical for stabilizing the transition states of the reactions.[39] Thus, catalysts need a special design in order to be able to perform asymmetric reactions in water. In the case of *L*-proline, the first water-compatible systems were achieved by connection of a hydrophobic fragment to the *L*-proline moiety. In water, the hydropobic parts will cluster, thereby creating aggregates where the catalysis occurs. A vast amount of *L*-proline derived water compatible organocatalysts has already been developed and two examples are shown in Figure 1.7.

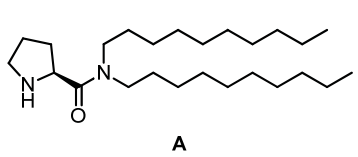

	A	B
Cat. loading (mol%)	10	10
	5 h	24 h, 0°C
Yield (%)	78	60
de (%)	68	90
ee (%)	22	99

Figure 1.7: Two different catalysts derived from *L*-proline catalyzing the aldol reaction in water (left) and their catalytic performance (right). A: Barbas-type catalyst.[37] B: Hayashi-type catalyst.[35]

1.2.2. Mechanism of *L*-proline catalysis

The vast majority of synthetic systems performing aldol reactions, including proline catalysis, proceed via an enamine mechanism similar to the type I aldolases in biological systems.[25] During the past decade, several mechanisms have been proposed for the proline-catalyzed aldol reaction. Agami *et al.*[40] proposed model I depicted in Figure 1.8 involving two proline moieties. However, more recent studies support a one-proline model (e.g. Figure 1.8 II).[41,42] List and coworkers, for example, reported "kinetic and stereochemical evidence for the involvement of only one proline molecule in the transition states." [43] Although the single-proline-mechanism has become the accepted mechanism, the exact catalytic cycle is still under debate.[44]

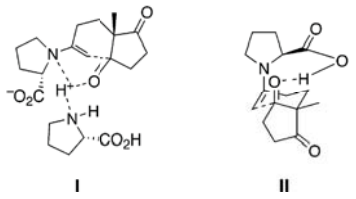

Figure 1.8: Possible transition states for an *L*-proline catalyzed aldol reaction.[45]

The currently accepted mechanism for the proline-catalyzed aldol reaction is depicted in Scheme 1.2. The aldol reaction proceeds via the enamine-based route, whereas the iminium intermediate **4** is able to yield the condensation-elimination product **8**.

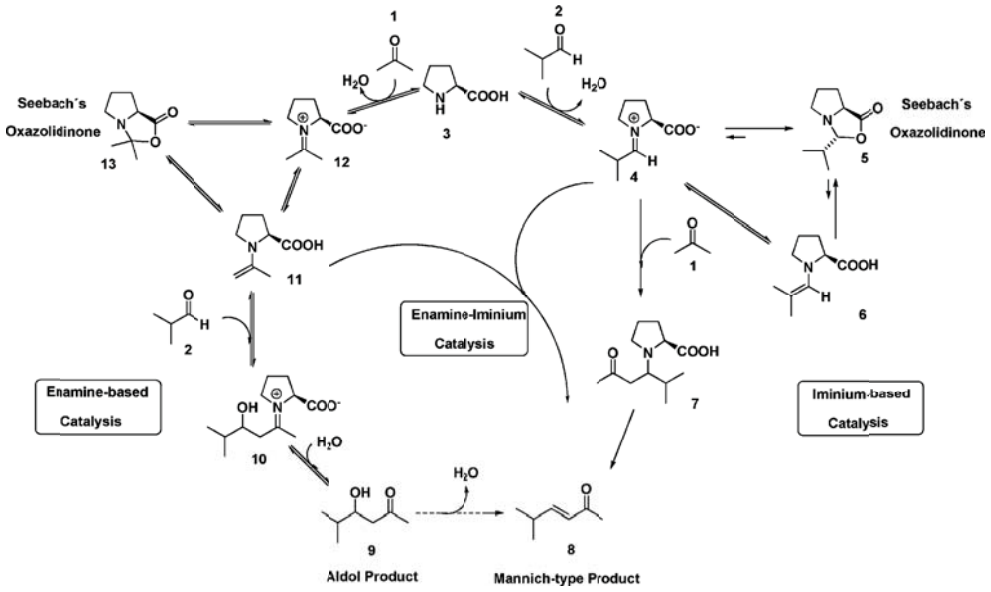

Scheme 1.2: Proposed mechanism for proline-catalyzed C-C bond formation.[42]

The role of the carboxylic acid functionality of the proline during catalysis is still a subject of discussion. List hypothesized that proline acts not only act as an enamine catalyst, but also brings with it its own Brønsted-acid co-catalyst. So, the acid is hypothesized to act as a general-purpose Brønsted co-catalyst, replacing the several acid/base functional groups involved in the aldolase mechanism.[46] On the contrary, Cheng and coworkers claimed that only the pyrrolidine ring in *L*-proline is required for aldol reactions in micelles and the carboxylic acid group is not involved.[47]

The configuration of the *L*-proline catalyzed aldol adduct can be rationalized by visualization of the transition state. Since the enamine intermediate can be formed in both the *anti*- and *syn*-configuration, and the aldehyde can approach at two faces, four different transition state complexes are possible. The most probable Zimmerman–Traxler-type chair-like transition state leading to the *anti*-(*S*,*R*)-product is depicted in Scheme 1.3.[46]

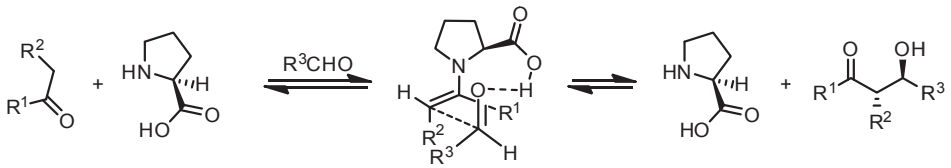

Scheme 1.3: Proposed transition state of the proline-catalyzed intermolecular aldol reaction.

1.3. Compartimentalized systems for catalysis

We already touched upon the importance to shield the proline moiety from the bulk water in order to accomplish efficient proline catalysis in water. The proline derivatives shown in Figure 1.7 rely on the formation of ill-defined aggregates causing the origin of their activity and selectivity to be poorly understood. In contrast, Nature protects reactions very elegantly from water by performing catalysis in a specific microenvironment in the interior of enzymes.

Scientists tried to mimic the natural approach, and designed compartimentalized systems able to form a similar hydrophobic microenvironment as observed in enzymes to shield the *L*-proline from the bulk water. Various highly-ordered compartimentalized systems are already reported in literature, including dendrimers,[48] amphiphilic polymers,[49] hydrogels,[50] and micelles.[51]

One recent example of an *L*-proline based enzyme mimic able to form a specific microenvironment is developed by O'Reilly and coworkers. *L*-proline was incorporated into the hydrophobic segment of amphiphilic block copolymers giving efficient polymeric nanoreactors for aldol reactions in water.[49] The assembled spherical-core shell structures were shown to have good catalytic properties, attributed to the ability of the nanostructures to effectively concentrate the reagents in the catalytically active micelle core. In further research, synthesis of *L*-proline functionalized hydrophobic nanogel particles (Figure 1.9) revealed the importance of local core environment design, since better enantioselectivities were obtained for increasing core hydrophobicity.[52]

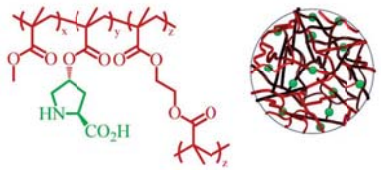

Cat. loading	1 mol%
	24 h
Yield	73%
de	94%
ee	99%

Figure 1.9: Molecular structure of the *L*-proline functionalized cross-linked poly(methyl methacrylate) polymer (left), schematic representation of the *L*-proline functionalized nanogel particles (middle) and the catalytic performance of the system (right).[52]

A promising approach allowing for more control over the formation of a specific microenvironment and positioning of the *L*-proline was recently developed in our group and is based on single-chain polymeric nanoparticles (SCPN). A methyl methacrylate-based polymer was functionalized with oligo(ethylene glycol) side chains to ensure solubility, and BTAs that are able to self-assemble in water. The polymer folds in water, driven by the hydrophobicity of the polymer backbone in combination with self-assembly of the BTAs, thereby forming an SCPN witch an ordered hydrophobic core.[53] Free BTAs functionalized with an *L*-proline moiety can be captured in the BTA stacks in the hydrophobic core of these well-defined compartmentalized architectures, thereby creating catalytically active SCPNs in water (Figure 1.10).[54]

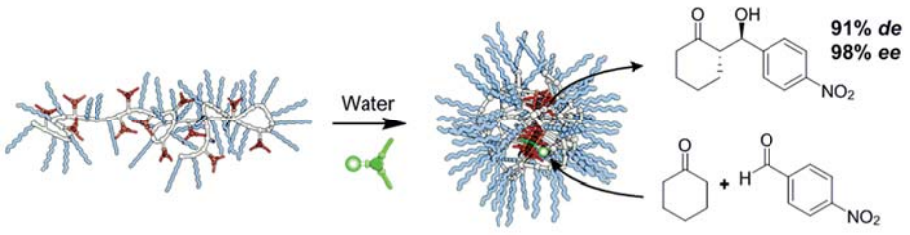

Figure 1.10: Schematic representation of the formation of SCPNs and the incorporation of functionalized BTAs.[54]

By serendipity, BTA-*L*-proline moieties (Figure 1.11 A) in absence of the SCPN were found to form highly active and stereoselective aggregates in water after a temperature treatment.[54] This temperature treatment is hypothesized to promote a conformational change in the supramolecular polymers (Figure 1.11 B) as revealed by a differently shaped CD spectrum (Figure 1.11 C). This conformational change is ultimately expressed in higher reaction rates.

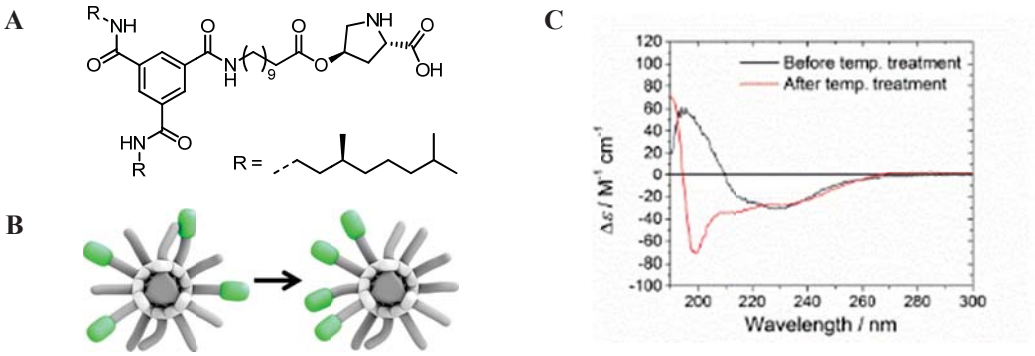

Figure 1.11: A: Molecular structure of catalytic BTA. B: Proposed reorganization of the L-proline moieties within the BTA stack caused by the temperature treatment. C: CD spectra of BTA-*L*-proline (c = 5 x 10^{-5} M, l = 5 mm) in water at room temperature before (black) and after (red) temperature treatment.

1.3.1. Close proximity of catalysts

The system described in the previous section where better catalytic activity is obtained if multiple catalytic units are present in close proximity is not unique. Stupp and coworkers reported a nanofiber formed by the aggregation of peptide amphiphiles showing a hydrolysis rate enhancement due to high density presentation of reactive sites with high internal order.[55]

In the field of proline catalysis, there has been little research into organization of multiple proline units in supramolecular systems. However, Miravet *et al.* reported an *L*-proline-derived low molecular weight gelator that is only efficient in its aggregated state (Figure 1.12).[56] Formation of the self-assembled fibrillar networks in nitroethane is associated to a basicity boost resulting in a sharp change in catalytic activity. The reversible nature of the gels allows for tuning of the catalytic activity by minor temperature changes.

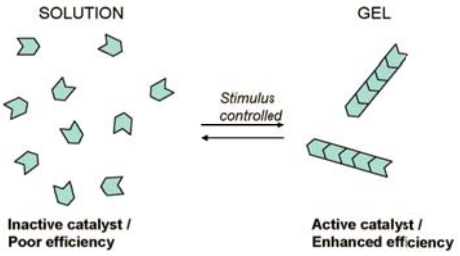

Figure 1.12: An *L*-proline-derived low molecular weight gelator was found to be efficient only upon aggregation into self-assembled fibrillar networks.[56]

Another system where close proximity of multiple proline moieties was shown to have a positive effect on the reactivity of the catalyst was reported by Zhao and coworkers. They reported found C_2-symmetric bisprolinamides to show more than doubled reactivity and a better asymmetric induction than the monoprolinamide counterparts.[57] The finding that multiple prolines in close proximity are more active is promising considering the design of an enzyme mimic whose catalytic activity can be tuned.

1.4. Aim of this work

In this research, we are aiming to use a BTA based system to develop an enzyme mimic. BTAs functionalized with a catalytic *L*-proline moiety are hypothesized to self-assemble in water into well-defined supramolecular stacks. Incorporation of the *L*-proline moieties into the hydrophobic core of these stacks is expected to yield a highly active and selective catalyst. The possibility to tune the local *L*-proline density in the stacks, allows for control over this well-defined system.

The design and synthesis of two different *L*-proline functionalized BTAs will be discussed in **chapter 2**.

In chapter 3, we will discuss the characterization of the new supramolecular system. Self-assembly is probed by infrared spectroscopy (IR), UV-Vis absorption spectroscopy, dynamic light scattering (DLS), short angle X-ray scattering (SAXS) and cryogenic transmission electron microscopy (cryo-TEM).

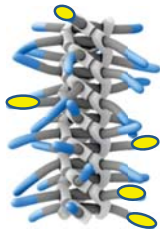

Figure 1.13: Schematic representation of functionalized BTAs incorporated into a BTA stack.

Chapter 4 explores the catalytic activity of the designed system (Figure 1.13). The possibility to dilution the local *L*-proline concentration in the assemblies allows to investigate the hypothesis that *L*-proline moieties in close proximity are more active and selective compared to catalytic units in a highly diluted fashion.

1.5. References

(1) Richter, J. P. *The Literary Works of Leonardo da Vinci*; Phaidon: Oxford, 1977.
(2) Festo AG & Co. KG. SmartBird – bird flight deciphered http://www.festo.com/cms/en_corp/11369_11378.htm#id_11378 (accessed Jul 7, 2014).
(3) Laio, A. Protein folding by atomistic simulations http://people.sissa.it/~laio/Research/Res_folding.php (accessed Aug 22, 2014).
(4) Lehn, J.-M. Nobel lecture: Supramolecular Chemistry – Scope and Perspectives Molecules – Supermolecules – Molecular Devices, 1987.

(5) Steed, J. W.; Atwood, J. L. *Supramolecular Chemistry*; 2nd ed.; John Wiley & Sons, Ltd: Chichester, 2009.
(6) Sessler, J. L.; Seidel, D. *Angew. Chem. Int. Ed.* **2003**, *42*, 5134–5175.
(7) Sijbesma, R. P.; Beijer, F. H.; Brunsveld, L.; Folmer, B. J. B.; Hirschberg, J. H. K. K.; Lange, R. F. M.; Lowe, J. K. L.; Meijer, E. W. *Science* **1997**, *278*, 1601–1604.
(8) Cantekin, S.; de Greef, T. F. A.; Palmans, A. R. A. *Chem. Soc. Rev.* **2012**, *41*, 6125–6137.
(9) Smulders, M. M. J.; Schenning, A. P. H. J.; Meijer, E. W. *J. Am. Chem. Soc.* **2008**, *130*, 606–611.
(10) De Greef, T. F. A.; Nieuwenhuizen, M. M. L.; Stals, P. J. M.; Fitié, C. F. C.; Palmans, A. R. A.; Sijbesma, R. P.; Meijer, E. W. *Chem. Commun.* **2008**, 4306–4308.
(11) Stals, P. J. M.; Haveman, J. F.; Martín-Rapún, R.; Fitié, C. F. C.; Palmans, A. R. A.; Meijer, E. W. *J. Mater. Chem.* **2009**, *19*, 124–130.
(12) Matsuura, K.; Murasato, K.; Kimizuka, N. *J. Am. Chem. Soc.* **2005**, *127*, 10148–10149.
(13) Lightfoot, M. P.; Mair, F. S.; Pritchard, R. G.; Warren, J. E. *Chem. Commun.* **1999**, 1945–1946.
(14) Stals, P. J. M.; Smulders, M. M. J.; Martín-Rapún, R.; Palmans, A. R. A.; Meijer, E. W. *Chem. – Eur. J.* **2009**, *15*, 2071–2080.
(15) Cantekin, S.; Balkenende, D. W. R.; Smulders, M. M. J.; Palmans, A. R. A.; Meijer, E. W. *Nat. Chem.* **2011**, *3*, 42–46.
(16) Brunsveld, L.; Schenning, A. P. H. J.; Broeren, M. A. C.; Janssen, H. M.; Vekemans, J. A. J. M.; Meijer, E. W. *Chem. Lett.* **2000**, *29*, 292–293.
(17) Leenders, C. M. A.; Albertazzi, L.; Mes, T.; Koenigs, M. M. E.; Palmans, A. R. A.; Meijer, E. W. *Chem. Commun.* **2013**, *49*, 1963–1965.
(18) Albertazzi, L.; Zwaag, D. van der; Leenders, C. M. A.; Fitzner, R.; Hofstad, R. W. van der; Meijer, E. W. *Science* **2014**, *344*, 491–495.
(19) Albertazzi, L.; Martinez-Veracoechea, F. J.; Leenders, C. M. A.; Voets, I. K.; Frenkel, D.; Meijer, E. W. *Proc. Natl. Acad. Sci.* **2013**, *110*, 12203–12208.
(20) Yang, X.; Zhang, G.; Zhang, D. *J. Mater. Chem.* **2011**, *22*, 38–50.
(21) Yuan, W.; Zou, H.; Guo, W.; Shen, T.; Ren, J. *Polym. Chem.* **2013**, *4*, 2658–2661.
(22) Houk, K. N.; List, B. *Acc. Chem. Res.* **2004**, *37*, 487–487.
(23) Dondoni, A.; Massi, A. *Angew. Chem. Int. Ed.* **2008**, *47*, 4638–4660.
(24) Hajos, Z. G.; Parrish, D. R. *J. Org. Chem.* **1974**, *39*, 1615–1621.
(25) Trost, B. M.; Brindle, C. S. *Chem. Soc. Rev.* **2010**, *39*, 1600–1632.
(26) Jarvo, E. R.; Miller, S. J. *Tetrahedron* **2002**, *58*, 2481–2495.
(27) List, B.; Lerner, R. A.; Barbas, C. F. *J. Am. Chem. Soc.* **2000**, *122*, 2395–2396.
(28) Pihko, P. M.; Laurikainen, K. M.; Usano, A.; Nyberg, A. I.; Kaavi, J. A. *Tetrahedron* **2006**, *62*, 317–328.
(29) Dalko, P. I.; Moisan, L. *Angew. Chem. Int. Ed.* **2004**, *43*, 5138–5175.
(30) Giacalone, F.; Gruttadauria, M.; Agrigento, P.; Noto, R. *Chem. Soc. Rev.* **2012**, *41*, 2406–2447.
(31) Li, S.; Wu, C.; Long, X.; Fu, X.; Chen, G.; Liu, Z. *Catal. Sci. Technol.* **2012**, *2*, 1068–1071.
(32) Zotova, N.; Franzke, A.; Armstrong, A.; Blackmond, D. G. *J. Am. Chem. Soc.* **2007**, *129*, 15100–15101.
(33) Blackmond, D. G.; Armstrong, A.; Coombe, V.; Wells, A. *Angew. Chem. Int. Ed.* **2007**, *46*, 3798–3800.
(34) Raj, M.; Singh, V. K. *Chem. Commun.* **2009**, 6687–6703.
(35) Hayashi, Y.; Aratake, S.; Okano, T.; Takahashi, J.; Sumiya, T.; Shoji, M. *Angew. Chem. Int. Ed.* **2006**, *45*, 5527–5529.
(36) Hayashi, Y.; Sumiya, T.; Takahashi, J.; Gotoh, H.; Urushima, T.; Shoji, M. *Angew. Chem. Int. Ed.* **2006**, *45*, 958–961.
(37) Mase, N.; Nakai, Y.; Ohara, N.; Yoda, H.; Takabe, K.; Tanaka, F.; Barbas, C. F. *J. Am. Chem. Soc.* **2006**, *128*, 734–735.
(38) Delaney, J. P.; Henderson, L. C. *Adv. Synth. Catal.* **2012**, *354*, 197–204.
(39) Lindström, U. M. *Chem. Rev.* **2002**, *102*, 2751–2772.

(40) Agami, C.; Meynier, F.; Puchot, C.; Guilhem, J.; Pascard, C. *Tetrahedron* **1984**, *40*, 1031–1038.
(41) List, B.; Hoang, L.; Martin, H. J. *Proc. Natl. Acad. Sci. U. S. A.* **2004**, *101*, 5839–5842.
(42) Domínguez de María, P.; Bracco, P.; Castelhano, L. F.; Bargeman, G. *ACS Catal.* **2011**, *1*, 70–75.
(43) Hoang, L.; Bahmanyar, S.; Houk, K. N.; List, B. *J. Am. Chem. Soc.* **2002**, *125*, 16–17.
(44) Nielsen, M.; Worgull, D.; Zweifel, T.; Gschwend, B.; Bertelsen, S.; Jørgensen, K. A. *Chem. Commun.* **2010**, *47*, 632–649.
(45) Saito, S.; Yamamoto, H. *Acc. Chem. Res.* **2004**, *37*, 570–579.
(46) List, B. *Acc. Chem. Res.* **2004**, *37*, 548–557.
(47) Peng, Y.-Y.; Ding, Q.-P.; Li, Z.; Wang, P. G.; Cheng, J.-P. *Tetrahedron Lett.* **2003**, *44*, 3871–3875.
(48) Wu, Y.; Zhang, Y.; Yu, M.; Zhao, G.; Wang, S. *Org. Lett.* **2006**, *8*, 4417–4420.
(49) Lu, A.; Cotanda, P.; Patterson, J. P.; Longbottom, D. A.; O'Reilly, R. K. *Chem. Commun.* **2012**, *48*, 9699–9701.
(50) Rodríguez-Llansola, F.; Miravet, J. F.; Escuder, B. *Chem. Commun.* **2009**, 7303–7305.
(51) Lipshutz, B. H.; Ghorai, S. *Org. Lett.* **2012**, *14*, 422–425.
(52) Lu, A.; Moatsou, D.; Longbottom, D. A.; O'Reilly, R. K. *Chem. Sci.* **2013**, *4*, 965.
(53) Huerta, E.; Stals, P. J. M.; Meijer, E. W.; Palmans, A. R. A. *Angew. Chem. Int. Ed.* **2013**, *52*, 2906–2910.
(54) Huerta, E.; van Genabeek, B.; Stals, P. J. M.; Meijer, E. W.; Palmans, A. R. A. *Macromol. Rapid Commun.* **2014**, *35*, 1320–1325.
(55) Guler, M. O.; Stupp, S. I. *J. Am. Chem. Soc.* **2007**, *129*, 12082–12083.
(56) Rodríguez-Llansola, F.; Escuder, B.; Miravet, J. F. *J. Am. Chem. Soc.* **2009**, *131*, 11478–11484.
(57) Samanta, S.; Liu, J.; Dodda, R.; Zhao, C.-G. *Org. Lett.* **2005**, *7*, 5321–5323.

Chapter 2 Synthesis of *L*-proline functionalized benzene-1,3,5-tricarboxamides

2.1. Introduction

This chapter deals with the design and synthesis of new *L*-proline functionalized water soluble BTAs. Starting from the general design of the water soluble BTA **3** consisting of a BTA core as central hydrogen bonding unit, aliphatic chains to shield the hydrophobic core and a tail consisting of hydrophilic tetraethylene glycol to ensure solubility,[1] two new BTAs were designed. In **1** (Figure 2.1), three *L*-proline moieties are coupled *via* an amide bond to the exterior of the three tails of the BTA, yielding a C_3 symmetric functionalized BTA. The self-assembly behavior of this BTA is expected to be unaffected by the functionalization, since the functionalization constitutes a relatively small change of the original BTA design. Another advantage of this first target molecule is its relatively easy synthesis.

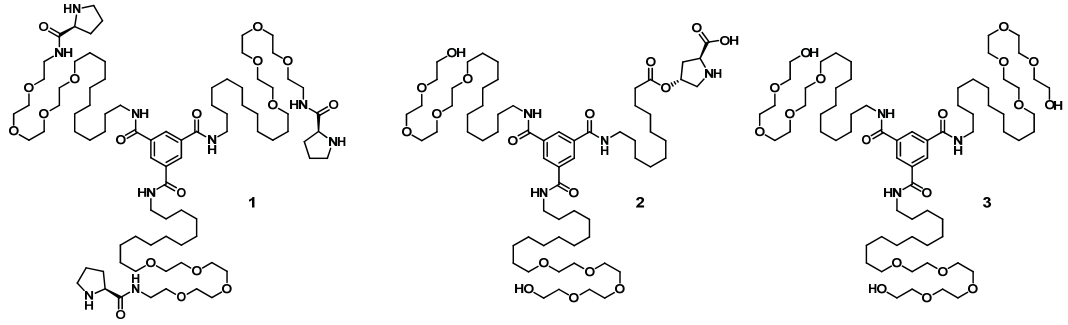

Figure 2.1: Chemical structures of water soluble, *L*-proline functionalized BTAs 1 and 2 as well as the unfunctionalized hydroxy BTA 3.

Next to BTA **1**, we also designed a second functionalized BTA: **2** bears two unmodified tails and one tail consisting of a hydrophobic carbon spacer with an *L*-proline moiety directly attached. Omission of the ethylene glycol spacer is hypothesized to allow for easy incorporation of the *L*-proline into the hydrophobic interior of the BTA stacks, thereby improving the shielding of the *L*-proline from the bulk water. Furthermore, the acid functionality which might be beneficial for efficient catalysis[5] will be preserved in **2**. The combination of those two changes is expected to ultimately lead to a more active and selective catalyst than **1**.[3–5] However, in **2** (and to a lesser extend in **1** as well), some major changes to the original design of **3** are made: functional groups are introduced and **2** contains only two ethylene glycol moieties. These changes might affect self-assembly of these molecules and can even result in loss of the self-assembling properties. The consequences of these changes on the self-assembly will be discussed in detail in chapter 3.

2.2. Synthetic approach towards functionalized BTAs

The two main components of **1** are *L*-proline and a water soluble BTA derivative. Initially, we attempted coupling of *L*-hydroxyproline *via* an ether to **3**, but this did not the envisioned target compound. *L*-proline was coupled to the BTA *via* an amide instead. On the contrary, the synthesis of mono-functionalized **2** requires a different approach. A hydrophobic spacer was functionalized with *L*-hydroxyproline and subsequently coupled to an asymmetric BTA derivative. Herein, we describe the successful synthesis of **1** and **2**.

2.2.1. Attempted ether coupling of *L*-hydroxyproline

The first approach to synthesize a BTA functionalized with *L*-proline on the exterior, as envisioned for BTA **1**, was to couple *L*-hydroxyproline *via* an ether bond to **3**. In order to achieve this functionalization, the Finkelstein reaction was used to tosylate the alcohols on the periphery of **3** and subsequently convert the tosyl groups into the iodide (**5**). In the last step, we tried to couple the *L*-hydroxyproline by using sodium hydride to deprotonate the alcohol functionality and thereby enable nucleophilic substitution of the iodide with the *L*-hydroxyproline. Surprisingly, the expected nucleophilic substitution did not occur, but elimination of the iodide was observed instead, yielding an alkene functionalized BTA (**8**). This is evidenced by the ^{1}H NMR spectrum in Figure 2.2 by the presence of peaks around 6.48, 4.17 and 3.99 ppm and their corresponding fine splitting pattern (three double doublets). The identity of the compound was confirmed by IR, ^{13}C NMR and MALDI-TOF. The high yield of this last reaction step (95%) and the high purity of the crude reaction mixture make this approach viable for the synthesis of (different) alkene functionalized BTAs. Although **8** is not useful for this project, it is a valuable starting compound for other BTA functionalizations e.g. enantioselective epoxidation yielding an epoxide[6] or hydroformylation followed by a Knoevnagel condensation to give three-carbon homologation.[7]

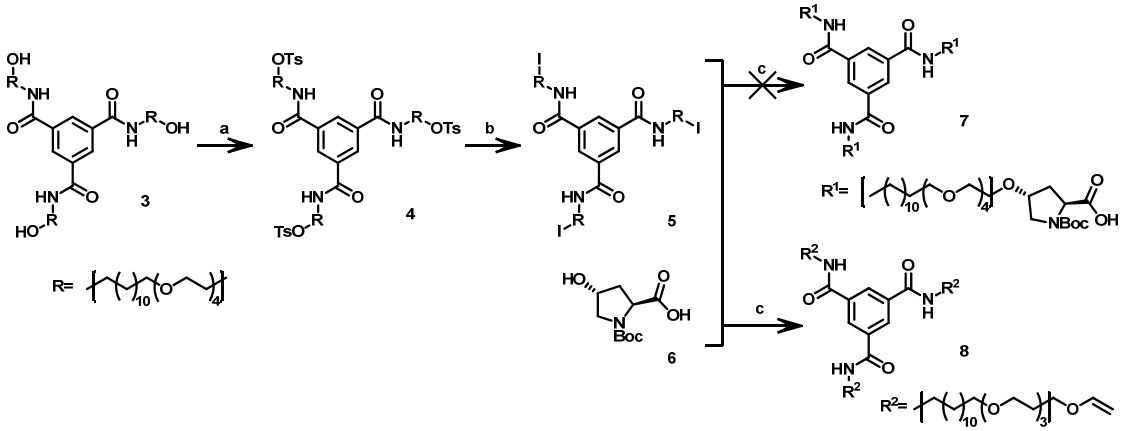

Scheme 2.1: Synthesis of an unexpected tris-alkene BTA Conditions: (a) p-TsCl, Me_3NHCl, $CHCl_3$, r.t., 20h, (79%); (b) NaI, acetone, reflux, 24h (quant.); (c) NaH, (2*S*,4*R*)-4-Hydroxyproline, DMF, r.t., 20h (95%).

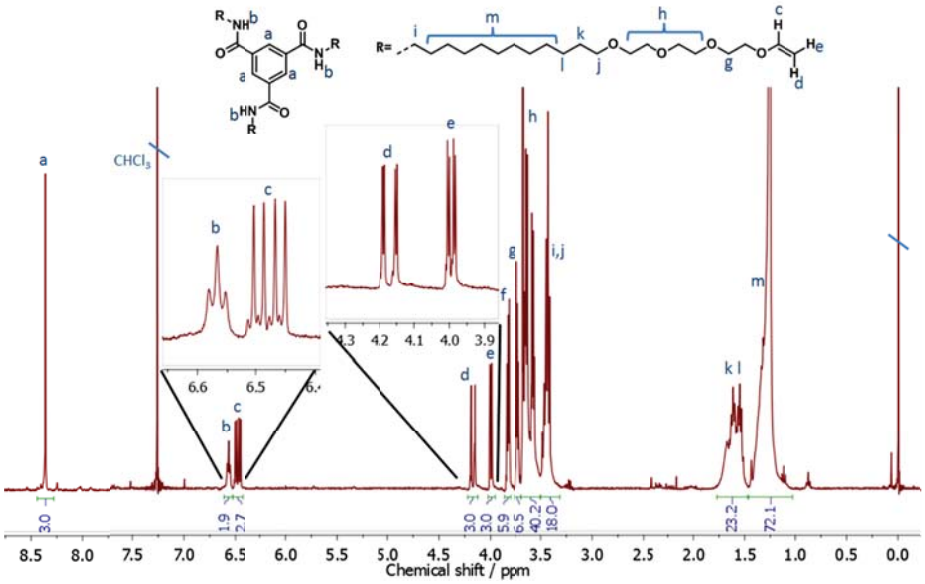

Figure 2.2: ^{1}H NMR spectrum (400 MHz, $CDCl_3$) of the unexpected tris-alkene BTA 8.

2.2.2. Synthesis of BTA-*L*-Pro **1**

Our initial approach to functionalize a BTA with *L*-proline moieties on the periphery was unsuccessful. Consequently, another approach was tested where the *L*-proline is coupled *via* the free acid to an amine BTA (**10**) upon the formation of an amide bond. A potential disadvantage of this approach is the loss of the free acid group on the *L*-proline, which is hypothesized by some groups to decrease the catalytic activity of the *L*-proline (see paragraph 2.1).[5]

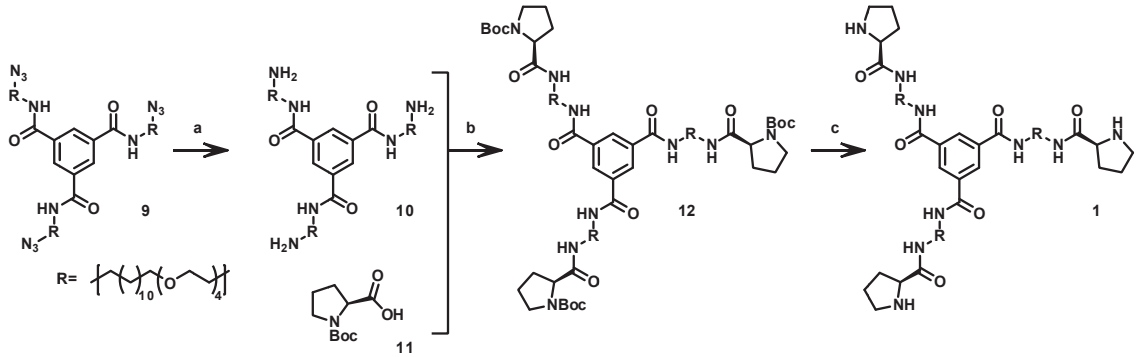

Scheme 2.2: Synthesis of the symmetrical *L*-proline functionalized BTA 1. Conditions: (a) PPh_3, H_2O, THF, 35°C, 72h (92%); (b) PyBOP, TEA, r.t., 18h (69%); (c) TFA, DCM, r.t., 24h (57%).

The azide-BTA **9** was kindly provided by Jolanda Spiering. Commonly, azides are converted to amines by catalytic hydrogenation. However, recently we encountered problems using this approach for the hydrogenation of azides. Therefore, we decided to use the Staudinger reduction as alternative.[8] The reaction shows excellent conversion. Removal of the excess of triphenylphosphine as well as the triphenylphosphine oxide formed during the reaction can easily be accomplished by a simple silica filtration.

After reduction of **9** to the amine BTA **10**, a PyBOP coupling was performed to couple the *L*-proline to the BTA. The PyBOP reagent (benzotriazol-1-yloxytri(pyrrolidino)-phosphonium hexafluorophosphate) uses a phosphonium group yielding to the advantage compared to triazoles that no guanidinium by-products are formed *via* reaction of the coupling reagent with amines.[9] Moreover, the particular improvement of PyBOP compared to BOP is that no carcinogenic hexamethylphosphoric triamide (HMPA) is formed.[10]

After coupling of the *L*-proline and purification of **12** by column chromatography, the Boc-group was cleaved by treatment with a 1:1 mixture of dichloromethane and trifluoroacetic acid. After extraction, target compound **1** was obtained in good purity and a yield of 57%. The aqueous phase was back-extracted to improve the yield of the reaction, but this was unsuccessful. The integrals in the ^{1}H NMR spectrum of **1** of the *L*-proline moieties and the BTA core in Figure 2.3 clearly show the presence of three *L*-proline moieties per BTA and absence of additional peaks at 1.4 ppm evidence complete removal of the protecting groups. ^{13}C NMR, LCMS, and IR were used to further confirm the identity and purity of the compound.

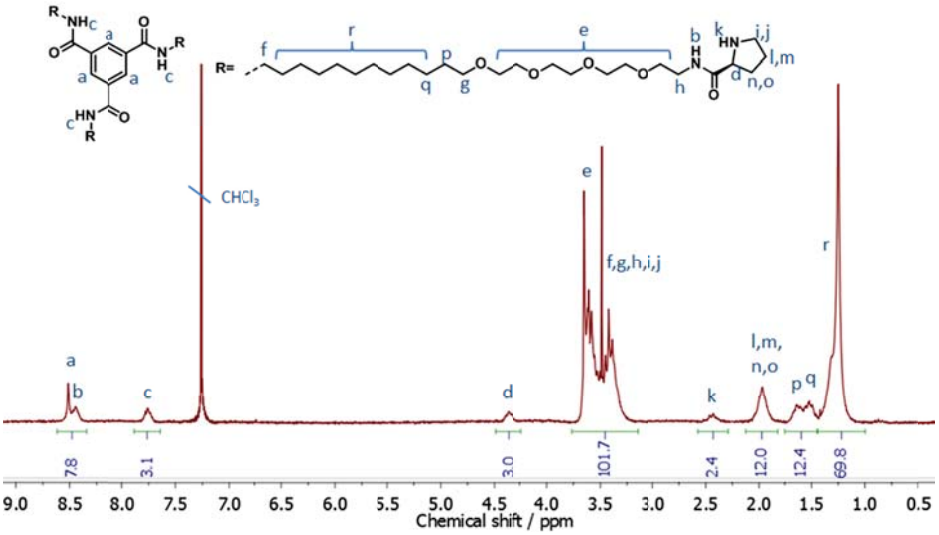

Figure 2.3: ^{1}H NMR spectrum (400 MHz, $CDCl_3$) of 1.

2.2.3. Synthesis of asymmetric BTA-*L*-Pro **2**

As already mentioned in the introduction, *L*-proline needs to be in a hydrophobic environment to allow for efficient catalysis.[2–4] In order to compare the catalytic performance of *L*-proline moieties attached to the exterior of the molecular structure as in **1** to *L*-proline moieties attached directly to the hydrophobic spacer, we developed BTA **2**. For the synthesis of **2**, we envision two possible, fundamentally different approaches: connection of the hydrophobic spacer to the BTA prior to the coupling of the *L*-hydroxyproline or linking of the hydrophobic spacer to the *L*-hydroxyproline and subsequent coupling to the BTA. The second approach was chosen (Scheme 2.3), due to its higher

versatility; it allows for the synthesis of various spacers that can be coupled to the same intermediate **13**.

In the design of **2**, the hydrophobic spacer to which the *L*-proline is coupled consists of 11 carbon atoms, whereas a C_{12} spacer is more commonly used in these types of BTAs. The C_{11} spacer was preferred in this case for the synthesis of **14** due to the faster availability and lower costs. Furthermore, we expect the supramolecular behavior of **2** to be unaffected by this choice, since Imke Pijpers showed self-assembly in water of BTAs bearing either a C_{11} and a C_{12} spacer. The protected *L*-hydroxyproline **17** was coupled to the C_{11} spacer *via* an ester bond, since introduction of an ester bond can be done in mild conditions, leaving the relatively labile protecting groups of the *L*-hydroxyproline unaffected.

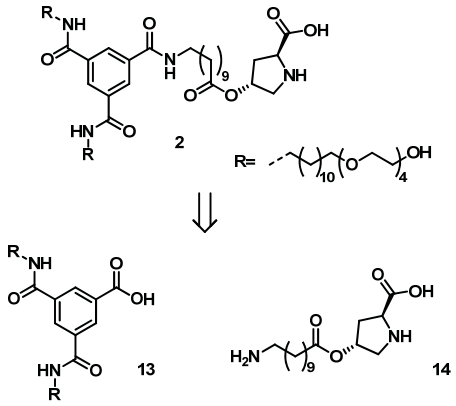

Scheme 2.3: Retrosynthetic approach for the synthesis of 2.

The two functional groups of *L*-hydroxyproline, a carboxylic acid and an amine, must be protected to be able to couple the *L*-hydroxyproline to the hydrophobic spacer without self-condensation or other side reactions. The effort of protecting the amine functionality was saved by buying commercially available *N*-Boc-protected *trans*-4-hydroxy-*L*-proline **16**. The acid was protected as the corresponding *tert*-butyl ester, enabling simultaneous removal of both protecting groups in the final step in one simple acid treatment step.[11]

The selective esterification of the carboxylic acid of *N*-Boc-*trans*-4-hydroxy-*L*-proline **16** was achieved with an *O*-*tert*-butyl isourea derivative **15** (Scheme 2.4)[12] kindly provided by Bas van Genabeek. Treatment of *N*-Boc-*trans*-4-hydroxy-*L*-proline **16** with this isourea derivative in THF at 60°C afforded the desired twofold protected *L*-proline **16** in 76% yield.

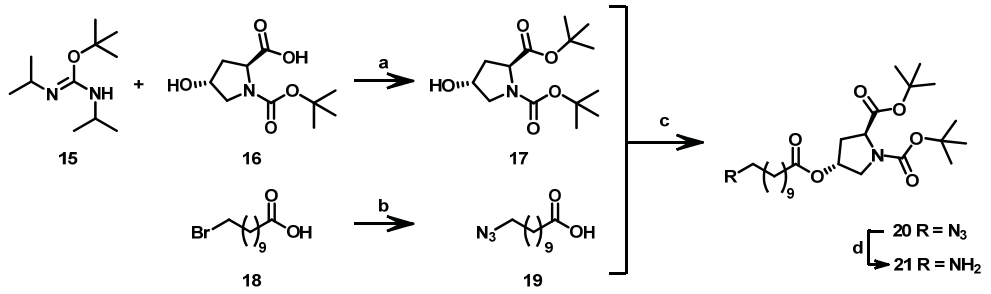

Scheme 2.4: Synthesis of *L*-proline functionalized hydrophobic spacer. Conditions: (a) THF, 60°C, 21h (76%); (b) NaN_3, DMSO, r.t., 18h (89%); (c) EDC·HCl, DPTS, $CHCl_3$, r.t., 72h (59%); (d) PPh_3, H_2O, THF, 35°C, 72h (44%).

The bromine functionality in **18** was converted into the azide in good yield (89%) using sodium azide. Subsequently, the protected *L*-hydroxyproline **17** was coupled *via* a modified Steglich esterification.[13] In the standard Steglich coupling conditions, 4-dimethylaminopyridine (DMAP) is used as acyl transfer agent in order to suppress the formation of *N*-acylurea byproducts. These byproducts can be formed during an unwanted side reaction of the reactive *O*-acylisourea intermediate. However, Stupp *et al*. found even further suppression of the *N*-acylurea formation by the addition of DMAP as its 4-toluensulphonic acid salt (abbreviated as DPTS), resulting in better yields.[14] Therefore, DPTS was chosen as acyl transfer agent for the reaction.

In the last step, the azide **20** was converted into amine **21**, to allow coupling to the BTA. This was done using the Staudinger reduction discussed previously. Purification of the target compound over a small column seemed to yield the compound in good purity as evidenced by a clean ^{1}H NMR spectrum. Analysis by LCMS, however, showed oligomerisation taking place as shown in Figure 2.4. Upon attack of the free amine on the ester, an amide is formed and the *L*-proline is eliminated as displayed in Scheme 2.5. Since storage as the HCl salt in order to prevent further self-condensation is not possible for **21** due to the limited stability of the protecting groups, the compound was used immediately in the next step of the synthesis. Removal of the oligomers was achieved in the very last step of the synthesis and will be discussed in the corresponding paragraph.

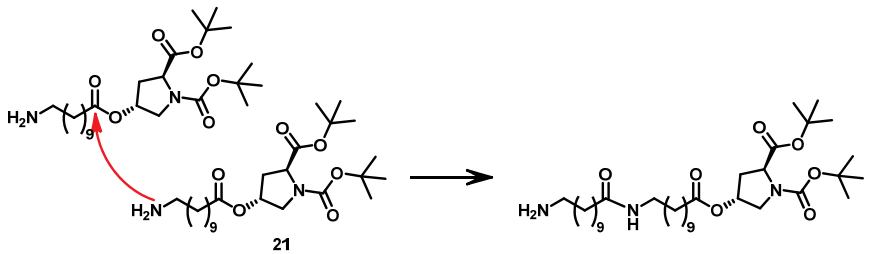

Scheme 2.5: Dimerization of the hydrophobic spacer 20.

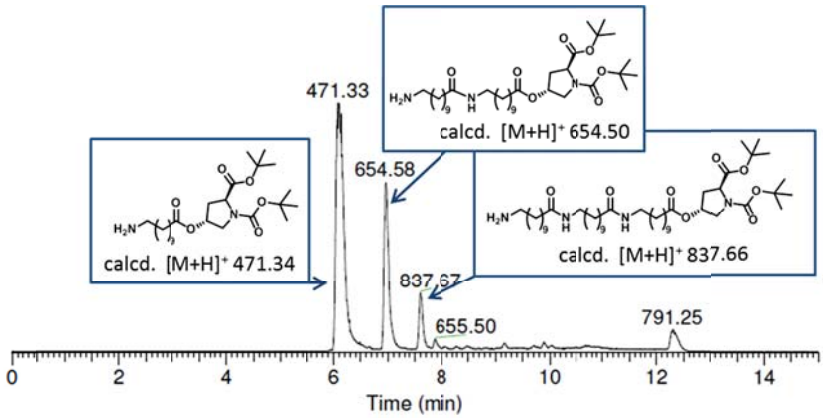

Figure 2.4: LCMS trace showing 15 and the self-condensated oligomers.

In the next step, the hydrophobic spacer needs to be coupled to the BTA *via* amide bond formation. Amide bond formation is usually achieved conveniently by conventional peptide-coupling reactions. In our specific case, this would imply coupling of the amine in **21** to the acid in BTA **13**. However, problems arise due to the presence of alcohol groups in **13** which can react with an acid, resulting in undesirable ester formation. This problem can be circumvented in two ways: synthesis of the benzyl-protected variant of **13** (*via* protection of **13** or starting from scratch) or by using a coupling agent able to promote amide bond formation in the presence of alcohols. Since Ronald Gosens kindly provided compound **13**, we saved a number of steps by choosing the second option. DMT-MM (4-(4,6-dimethoxy-(1,3,5)triazin-2-yl)-4-methyl-morpholiniumchloride), a triazine derivative, was chosen as coupling agent, since it enables synthesis of amide in the presence alcohols while minimizing ester formation compared to traditional coupling agents.[9] BTA **13** undergoes an S_NAr reaction yielding an activated ester which is subsequently displaced by the amine.[15] For this reaction, no additional base is required since *N*-methylmorpholine is formed during the first step. Furthermore, the workup is simplified because the triazinone by-product formed during the reaction can easily be removed by aqueous washing.

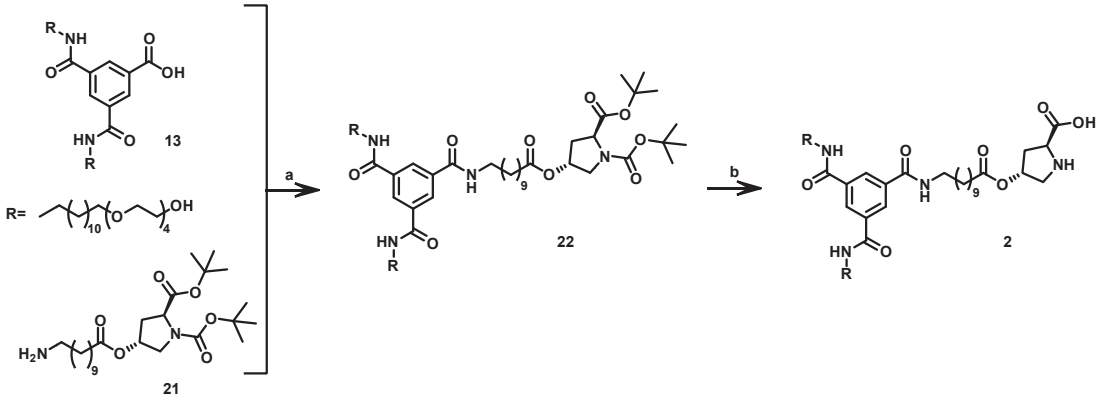

Scheme 2.6: Coupling of the hydrophobic spacer to the BTA. Conditions: (a) DMT-MM, DMF, r.t., 20h (35%); (b) TFA, DCM, r.t., 18h (70%).

Unfortunately, the yield of the DMT-MM coupling is low, which is likely caused by the low activity of the old DMT-MM batch. Nevertheless, compound **22** was obtained in good purity. The *tert*-butyl ester- and Boc-protecting groups were removed by treatment with a 1:1 mixture of dichloromethane and trifluoracetic acid. Reversed phase column chromatography in a water/acetonitrile mixture yielded pure BTA **2** as depicted in the ^{1}H NMR spectrum in Figure 2.5. This reversed phase column allowed for separation of the BTAs containing a 'double spacer,' as shown in Scheme 2.5 and discussed previously, and our target compound **2**. BTA **2** was obtained in high purity, as depicted in Figure 2.6. The removal of the unwanted BTA adducts explains the apparent relative low yield of this last deprotection step.

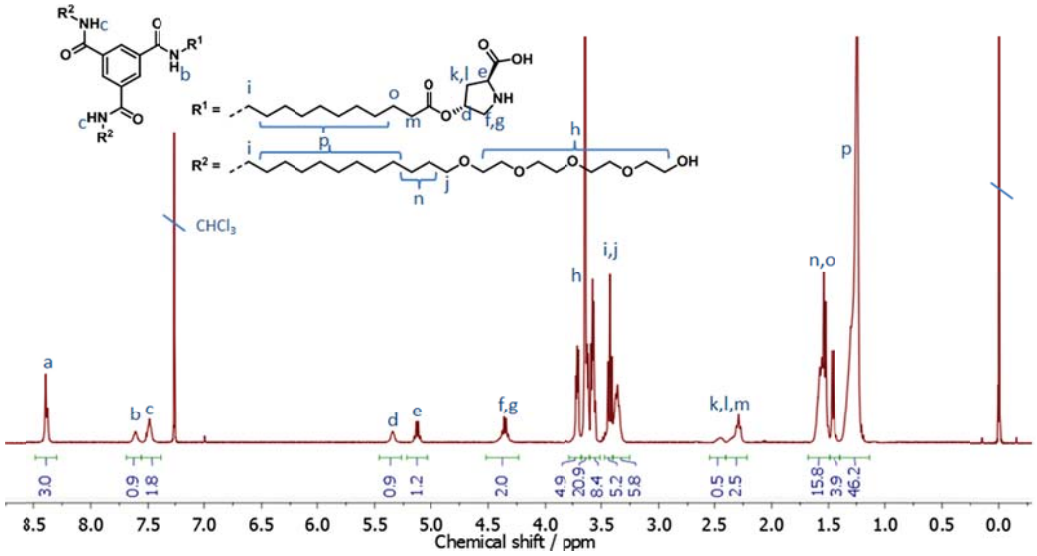

Figure 2.5: ^{1}H NMR spectrum (400 MHz, $CDCl_3$) of 2.

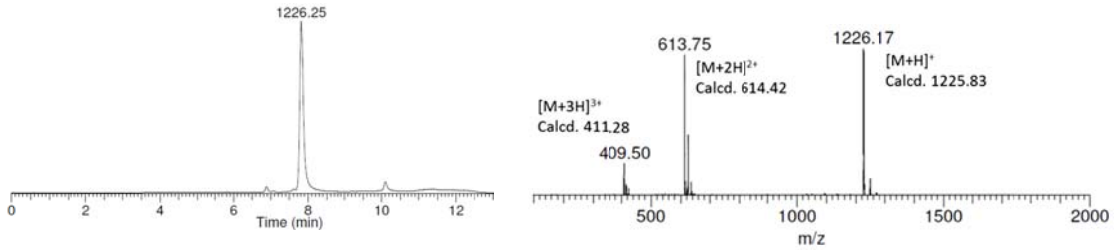

Figure 2.6: LCMS trace of pure compound 18 (left) and mass trace of the peak (right).

2.3. Conclusion

Two *L*-proline functionalized BTAs (**1** and **2**) were designed and successfully synthesized. Our initial attempt to couple *L*-hydroxyproline to BTA **3** *via* an ether bond did not yield the desired BTA, but an alkene functionalized BTA (**8**) which might be a valuable starting compound for other BTA functionalizations. The symmetric, three times substituted BTA **1** was obtained by coupling of the acid of *L*-proline *via* an amide bond to the periphery of amine BTA **9** in three steps with an overall

yield of 36% starting from the azide-BTA **8.** The asymmetric BTA **2** was obtained by coupling of a carbon spacer functionalized with *L*-hydroxyproline *via* an amide bond to the BTA core. This synthesis was performed in six steps with an overall yield of 4.8% starting from the BTA intermediate **13** and commercially available *trans*-4-hydroxy-*L*-proline. The low overall yield is partly caused by a side-reactions that resulted in oligomerisation of **21**. This oligomerisation can be circumvented by coupling of the hydrophobic spacer to the BTA prior to coupling of the *L*-proline derivative **17**.

Both compounds are obtained in high purity and can be utilized for further exploration of the designed catalytic system. Their different molecular designs, **1** having three proline moieties at the periphery connected *via* an amide bond and **2** bearing one proline moiety in the hydrophobic interior connected *via* an ester bond, are expected to result in different behavior.

2.4. Experimental section

2.4.1. Materials

All reagents were purchased from Sigma-Aldrich or Acros Organics and used as received, unless otherwise specified. All solvents were purchased from Biosolve. Chloroform and THF were dried over 4Å molecular sieves before use. Triethylamine was dried and stored over KOH pellets. Deuterated compounds were obtained from Cambridge Isotopes Laboratories and stored over 4Å molecular sieves. All reactions were carried out under argon atmosphere unless stated otherwise. Reactions were followed by thin-layer chromatography (TLC) using 60-F254 silica gel plates from Merck and visualized by UV light at 254 nm and/or ninhydrin-, bromocresol green-, and cerium molybdate staining. Flash column chromatography was performed on a Biotage Isolera II Chromatography system using SNAP columns or a Grace Reverleris X2 system using Grace silica flash cartridges. Reversed phase column chromatography was achieved using a reversed phase KP-C_{18}-HS SNAP column or a Reverleris C18 reversed-phase flash cardridge.

DMT-MM was synthesized according to literature procedures.[16,17]

2.4.2. Instrumentation

All ^{1}H-NMR and ^{13}C-NMR spectra were recorded on a Varian Mercury Vx 400 MHz and/or a Varian 400 MHz (400 MHz for ^{1}H-NMR and 100 MHz for ^{13}C-NMR). Proton chemical shifts are reported in ppm (δ) downfield from trimethylsilane (TMS) using the resonance frequency of the deuterated solvent as the internal standard. Peak multiplicity is abbreviated as s: singlet; d: doublet; t: triplet; q: quartet; sept: septet; m: multiplet; bs: broad singlet; brsept: broad septet. Carbon chemical shifts are reported in ppm (δ) downfield from TMS using the resonance frequency of the deuterated solvent as the internal standard. Matrix assisted laster absorption/ionization mass spectra were obtained on a PerSeptive Biosystems Voyager DE-PRO spectrometer using α-cyano-4-hydroxycinnamic acid (CHCA) or *trans*-2-[3-(4-*tert*-butylphenyl)-2-methyl-2-propenylidene]malononitrile (DCBT) as matrix. Infrared spectra were recorded using a Perkin Elmer Spectrum Two FT-IR spectrometer equipped with a Perkin Elmer Universal ATR Two Accessory. Freeze drying was achieved using a Salmenkipp Christ Alpha 2-4 LD Plus freeze dry system equipped with a Vacuubrand RC6 Chemistry Hybrid vacuum pump.

2.4.3. Synthetic procedures

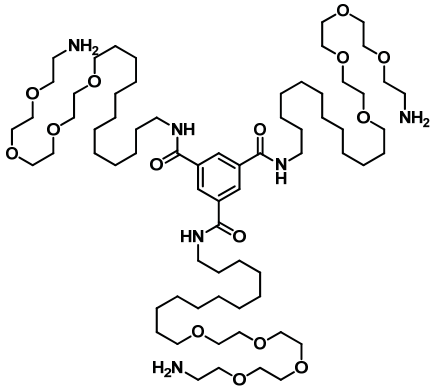

N1,N3,N5-tris(1-amino-3,6,9,12-tetraoxatetracosan-24-yl)benzene-1,3,5-tricarboxamide (**10**) A round bottom flask was charged with *N*1,*N*3,*N*5-tris(1-azido-3,6,9,12-tetraoxatetracosan-24-yl)benzene-1,3,5-tricarboxamide (**9**) (0.649 mmol, 0.885 g), triphenylphosphine (3.89 mmol, 1.01 g) and THF (4 ml). The solution was stirred overnight at 35°C. A mixture of water (1.2 ml) and THF (0.8 ml) was added and the solution was again stirred overnight at 35°C. The reaction mixture was concentrated *in vacuo* and purified by silica filtration (eluent chloroform/methanol, 95/5, v/v and chloroform/methanol/isopropylamine, 90/8/2, v/v). The desired compound was obtained as an white solid (0.784 g, 92%).

^{1}H NMR (400 MHz, $CDCl_3$): δ = 8.38 (s, 3H, Ar), 6.77 (m, 3H, C=ON<u>H</u>CH_2), 3.67–3.55 (m, 36H, O–$(CH_2)_2$–O), 3.50–3.40 (m, 18H, $CH_2C\underline{H}_2NHC$=O, $CH_2CH_2C\underline{H}_2O$), 2.85 (t, J^3 = 5.3 Hz, 6H, $CH_2C\underline{H}_2NH_2$), 1.66–1.48 (m, 12H, $CH_2C\underline{H}_2CH_2O$, $C\underline{H}_2CH_2CH_2O$), 1.42–1.22 (m, 48H, aliphatic). MALDI-TOF-MS: calcd. $[M + H]^+$ 1285.96, found 1286.00. FT-IR (ATR) ν (cm^{-1}): 3245, 3074, 2924, 2854, 2102, 1642, 1556, 1466, 1349, 1294, 1119, 1039, 939, 853, 723, 691, 646.

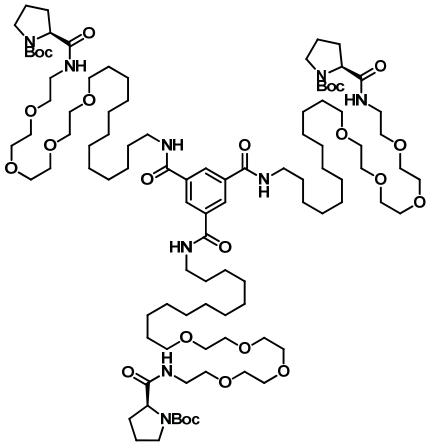

(2S,2'S,2''S)-tri-tert-butyl 2,2',2''-(28,28',28''-(benzene-1,3,5-triyl)tris(28-oxo-5,8,11,14-tetraoxa-2,27-diazaoctacosan-1-oyl))tris(pyrrolidine-1-carboxylate) (**12**) A round bottom flask was charged with (S)-1-(tert-butoxycarbonyl)pyrrolidine-2-carboxylic acid (0.586 g, 0.456 mmol), DIPEA (357 µl, 2.05 mmol) and chloroform (5 ml). *N*1,*N*3,*N*5-tris(1-amino-3,6,9,12-tetraoxatetracosan-24-yl)benzene-1,3,5-tricarboxamide (**10**) and (benzotriazol-1-yl-oxytripyrrolidinophosphonium hexafluorophosphate) (PyBOP, 0.783 g, 1.50 mmol) were added to the solution and the solution was stirred overnight at room temperature. The crude was concentrated *in vacuo* and purified by column

chromatography (eluent chloroform/methanol 100/0 to 93/7 v/v and dimethoxyethane/heptane 60/40 to 80/20). Yield = 0.590 g, 69%.

^{1}H NMR (400 MHz, $CDCl_3$): δ = 8.37 (s, 3H, Ar), 6.72 (m, 3H, Ar–C=ONHCH$_2$), 6.49 (b, 3H, CHC=ONHCH), 4.22 (m, 3H, C=ONHCH), 3.67–3.50 (m, 36H, O-(CH$_2$)$_2$-O), 3.50–3.29 (m, 24H, CH$_2$CH$_2$NHC=O, CH$_2$CH$_2$CH$_2$O, OCH$_2$CH$_2$NH, C=OCHNCH$_2$), 1.86 (m, 12H, C=OCHCH$_2$CH$_2$, C=OCHCH$_2$CH$_2$), 1.53 (m, 12H, CH$_2$CH$_2$CH$_2$O, CH$_2$CH$_2$CH$_2$O), 1.49–1.40 (m, 27H, CH$_3$C), 1.40–1.20 (m, 54H, NCHCH$_2$CH$_2$, aliphatic). ^{13}C NMR (100 MHz, $CDCl_3$) δ = 165.69, 135.24, 128.06, 76.68, 71.53, 70.63, 70.58, 70.46, 70.29, 70.02, 69.88, 40.34, 39.12, 29.57, 29.52, 29.47, 29.46, 29.43, 29.41, 29.23, 28.36, 26.93, 26.04. MALDI–TOF–MS: calcd. $[M + Na]^+$ 1899.28, found 1899.33. FT–IR (ATR) ν (cm^{-1}): 3320, 3075, 2925, 2855, 1663, 1536, 1453, 1393, 1366, 1285, 1256, 1163, 1120, 1039, 979, 922, 880, 861, 774, 706, 634, 592, 551.

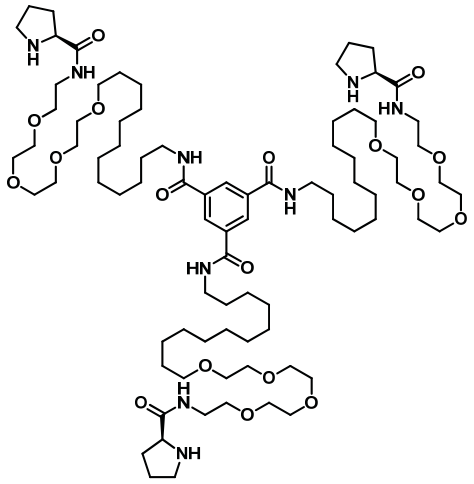

N1,N3,N5–tris(1–oxo–1–((S)–pyrrolidin–2–yl)–5,8,11,14–tetraoxa–2–azahexacosan–26–yl)benzene–1,3,5–tricarboxamide (**1**) A round bottom flask was charged with (2S,2'S,2''S)–tri–tert–butyl 2,2',2''–(28,28',28''–(benzene–1,3,5–triyl)tris(28–oxo–5,8,11,14–tetraoxa–2,27–diazaoctacosan–1–oyl))tris(pyrrolidine–1–carboxylate) (**12**) (228 mg, 0.314 mmol), 2 ml dichloromethane and 2 ml trifluoroacetic acid. The mixture was stirred overnight at room temperature. All the volatiles were removed *in vacuo* and the crude was dissolved in chloroform (15 ml) and washed with aq. NH_4Cl (2x 20 ml), dried over $MgSO_4$. The solvent was removed *in vacuo* and material was used without further purification. The desired compound was obtained as an off-white solid (95.3 mg, 56.7%).

^{1}H NMR (400 MHz, $CDCl_3$): δ = 8.52 (s, 3H, Ar), 8.48 (m, 3H, NHCHC=ONH), 7.79 (m, 3H, Ar–C=ONHCH$_2$), 4.41 (m, 3H, C=ONHCH), 3.67–3.51 (m, 36H, O-(CH$_2$)$_2$-O), 3.47–3.33 (m, 24H, CH$_2$CH$_2$NHC=O, CH$_2$CH$_2$CH$_2$O, OCH$_2$CH$_2$NH, C=OCHNHCH$_2$), 2.45 (m, 3H, C=OCHNH), 2.07–1.85 (m, 12H, C=OCHCH$_2$CH$_2$, C=OCHCH$_2$CH$_2$), 1.71–1.43 (m, 12H, CH$_2$CH$_2$CH$_2$O, CH$_2$CH$_2$CH$_2$O), 1.40–1.22 (m, 54H, NCHCH$_2$CH$_2$, aliphatic). ^{13}C NMR (100 MHz, $CDCl_3$) δ = 166.40, 135.08, 128.82, 71.40, 70.53, 70.44, 70.37, 69.99, 69.96, 69.32, 59.69, 46.59, 39.62, 30.49, 29.43, 29.24, 29.22, 29.16, 29.11, 26.92, 25.89, 24.71. LCMS: calcd. $[M+H]^+$ 1577.13, found 1577.00. FT–IR (ATR) ν (cm^{-1}): 3264, 3073, 2923, 2853, 2098, 1650, 1538, 1456, 1349, 1288, 1260, 1099, 1038, 942, 802, 750, 705, 664, 571.

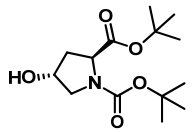

(2S,4R)–di–tert–butyl 4–hydroxypyrrolidine–1,2–dicarboxylate (**17**) A 100 ml round bottom flask was charged with trans–N–(tert–Butoxycarbonyl)–4–hydroxy–*L*–proline (1.51 g, 6.49 mmol) (**16**) and tetrahydrofuran (20 ml). A solution of (Z)–tert–butyl *N*,*N*′–diisopropylcarbamimidate (the isourea **15**) (2.00 g, 10 mmol, 1.5 eq.) in 10 ml tetrahydrofuran was added and the mixture was stirred at 60°C for 4 hours. Additional isourea (1.32 g, 6.5 mmol, 1 eq.) was added and stirring was continued overnight at 60°C. The formed white precipitate of urea was filtered off and the residue was washed with diethyl ether (10 ml). The organics were concentrated *in vacuo* yielding a bluish viscous oil. The crude was purified by column chromatography using heptane/EtOAc (70/30 to 40/60 v/v) as eluent yielding 1.41 g of the product (76%).

^{1}H NMR (400 MHz, $CDCl_3$): δ = 4.47 (bs, 1H, C<u>H</u>OH), 4.28 (m, 1H, C<u>H</u>C=O), [3.63 (d, J^3 = 4.4 Hz), 3.60 (d, J^3 = 4.3 Hz) 1H, NC<u>H</u>$_2$CHOH], [3.53 (d, J^3 = 11.6 Hz), 3.41(d, J^3 = 11.3 Hz) 1H, CHC<u>H</u>$_2$CH], 2.27 (m, 1H, HOCHC<u>H</u>$_2$), 2.05 (m, 1H, HOCHC<u>H</u>$_2$), 1.45 (m, 18H, C<u>H</u>$_3$). MALDI–TOF–MS: calcd. $[M+Na]^+$ 310.16, found 310.24. FT–IR (ATR) ν (cm^{-1}): 3442, 2978, 2935, 2880, 2079, 1740, 1701, 1674, 1393, 1366, 1255, 1219, 1148, 1086, 1053, 992, 938, 854, 771, 557, 468.

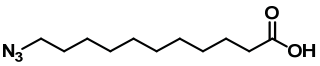

11–azidoundecanoic acid (**19**) In a round bottom flask, 11–bromoundecanoic acid (2.03 g, 7.65 mmol) (**18**) and sodium azide (0.813 g, 12.5 mmol) was dissolved in DMSO (70 ml) and stirred overnight at room temperature. The solution was quenched with 150 ml water. The product was extracted into ether (3x200 ml). The ether layers were combined, washed with acidified brine (350 ml), dried with Na_2SO_4 and the solvent was removed *in vacuo.* Yield = 1.52 g, 89%.

^{1}H NMR (400 MHz, $CDCl_3$): δ = 3.26 (t, J^3 = 6.9 Hz, 2H, N_3C<u>H</u>$_2CH_2$), 2.35 (t, J^3 = 7.5 Hz, 2H, C<u>H</u>$_2$COOH), 1.62 (m, 4H, CH_2C<u>H</u>$_2CH_2$COOH, C<u>H</u>$_2CH_2CH_2$COOH), 1.41–1.25 (m, 12H, aliphatic). ^{13}C NMR (100 MHz, $CDCl_3$) δ = 179.77, 51.48, 33.97, 29.38, 29.28, 29.18, 29.11, 29.01, 28.83, 26.70, 24.65. MALDI–TOF–MS: calcd. $[M - H]^-$ 226.16, found 226.20. FT–IR (ATR) ν (cm^{-1}): 2929, 2856, 2096, 1709, 1458, 1413, 1349, 1285, 1257, 1103, 936, 723, 640, 553, 485.

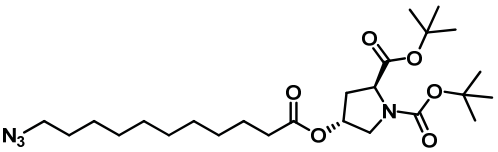

(2S,4R)–di–tert–butyl 4–((11–azidoundecanoyl)oxy)pyrrolidine–1,2–dicarboxylate (**20**) A round bottom flask was charged with 11–azidoundecanoic acid **19** (0.360 g, 1.589 mmol), the double protected proline **17** (0.494 g, 1.72 mmol), 4–(dimethylamino)pyridinium 4–toluenesulfonate (DPTS) (0.796 g, 2.70 mmol) and dry chloroform (10 ml). The solution was cooled in an ice/salt bath to below 0°C and a cooled solution of *N*–(3–Dimethylaminopropyl)–*N*′–ethylcarbodiimide hydrochloride (0.943 g, 4.92 mmol) in dry cholorform (3 ml) was added quickly. The clear solution was stirred at room temperature overnight. Then, the reaction mixture was transferred to a separatory funnel,

additional chloroform was added (30 ml), and the solution was washed with water (2x 40 ml) and brine (40 ml). The organic layer was dried over $MgSO_4$ and the solvent was removed *in vacuo*. The material was purified by column chromatography (eluent heptane/ethyl acetate 90/10 to 75/25 v/v) yielding the target compound (0.584 g, 74%).

^{1}H NMR (400 MHz, $CDCl_3$): δ = 5.25 (bs, 1H, C=OOC<u>H</u>), 4.23 (m, 1H, $CH_2C\underline{H}C$=O), 3.66 (m, 2H, $CHC\underline{H}_2N$), 3.25 (t, J^3 = 6.9 Hz, 2H, $N_3C\underline{H}_2$), 2.33 (m, 1H, $CHC\underline{H}_2CH$), 2.28 (t, J^3 = 7.5 Hz, 2H, $C\underline{H}_2C$=O), 2.17 (m, 1H, $CHC\underline{H}_2CH$), 1.70–1.53 (m, 4H, $CH_2C\underline{H}_2CH_2C$=O, $C\underline{H}_2CH_2CH_2C$=O), 1.53–1.39 (m, 18H, $C\underline{H}_3C$), 1.39–1.10 (m, 12H, aliphatic). ^{13}C NMR (100 MHz, $CDCl_3$) δ = 173.23, 171.62, 153.84, 81.39, 80.29, 71.61, 58.49, 51.99, 51.48, 36.70, 34.26, 29.40, 29.30, 29.19, 29.11, 29.05, 28.83, 28.33, 28.01, 27.94, 26.70, 24.82. MALDI–TOF–MS: calcd. $[M + Na]^+$ 519.32, found 519.31. FT–IR (ATR) ν (cm^{-1}): 2978, 2930, 2857, 2095, 1739, 1705, 1457, 1395, 1367, 1256, 1219, 1153, 1069, 995, 854, 771.

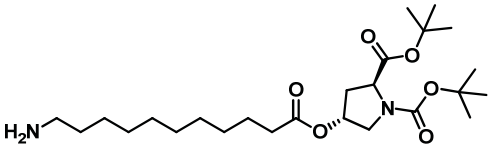

(2S,4R)–di–tert–butyl 4–((11–aminoundecanoyl)oxy)pyrrolidine–1,2–dicarboxylate (**21**) A 25 ml round bottom flask was charged with the proline functionalized carbon spacer **20** (0.541 g, 1.10 mmol), triphenylphosphine (570 mg, 2.17 mmol, 1.99 eq) and 8 ml tetrahydrofuran. The solution was stirred at 35°C overnight. A mixture of 2.4 ml water and 1.6 ml tetrahydrofuran was added and stirring was continued at 35°C overnight. The volatiles were removed *in vacuo* and the remaining water was removed on the freeze dryer. The crude was concentrated *in vacuo* and purified by column chromatography (eluent chloroform/methanol/triethylamine 100/0/0 to 91/7/2 v/v/v). Yield = 0.226 g, 44%. Oligomerisation of **21** yields a ~20% impurity (based on LCMS) as shown below.

^{1}H NMR (400 MHz, $CDCl_3$): δ = 5.25 (bs, 1H, C=OOC<u>H</u>), 4.25 (m, 1H, $CH_2C\underline{H}C$=O), 3.72–3.45 (m, 2H, $CHC\underline{H}_2N$), 2.67 (t, J^3 = 6.9 Hz, 2H, $H_2NC\underline{H}_2$), 2.34 (m, 1H, $CHC\underline{H}_2CH$), 2.28 (t, J^3 = 7.6 Hz, 2H, $C\underline{H}_2C$=O), 2.16 (m, 1H, $CHC\underline{H}_2CH$), 1.65–1.54 (m, 2H, $C\underline{H}_2CH_2C$=O), 1.50–1.38 (m, 18H, $CC\underline{H}_3$), 1.37–1.20 (m, 14H, aliphatic). ^{13}C NMR (100 MHz, $CDCl_3$) δ = 173.25, 171.62, 81.40, 80.29, 77.33, 77.22, 77.01, 76.70, 71.60, 58.49, 51.99, 42.25, 36.70, 34.27, 33.80, 29.55, 29.46, 29.38, 29.22, 29.07, 28.33, 28.01, 26.88, 24.84. MALDI-TOF: calcd. $[M + Na]^+$ 493.34, found 493.33. FT–IR (ATR) ν (cm^{-1}): 3314, 2977, 2927, 2854, 1740, 1705, 1560, 1458, 1397, 1367, 1256, 1220, 1160, 1068, 995, 937, 854, 771, 555.

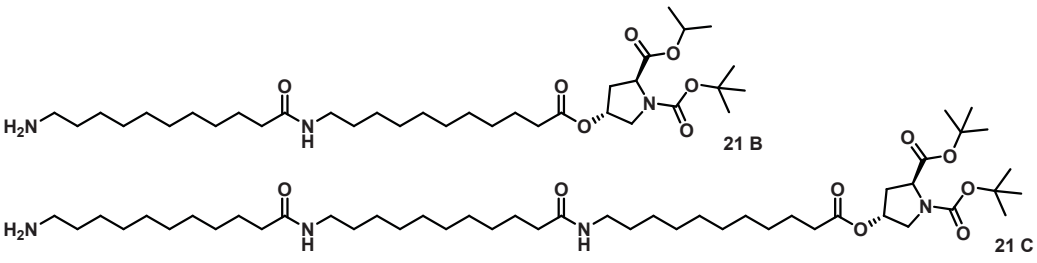

MALDI-TOF: calcd. [**21 B** + Na]$^+$ 676.49, found 676.47; [**21 C** + Na]$^+$ 859.65, found 859.63. LCMS: calcd. [**21 B** + H]$^+$ 654.50, found 654.50; [**21 C** + H]$^+$ 837.66, found 837.67.

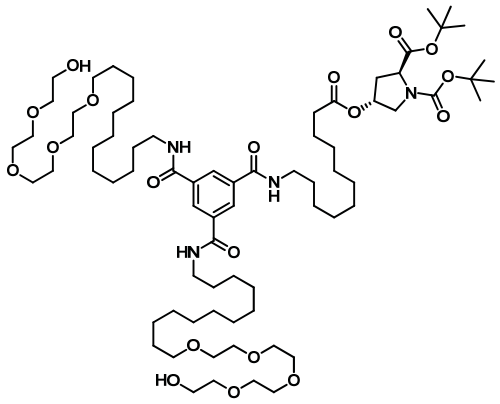

(2S,4R)–di–tert–butyl 4–((11–(3,5–bis((1–hydroxy–3,6,9,12–tetraoxatetracosan–24–yl)carbamoyl)benzamido)undecanoyl)oxy)pyrrolidine–1,2–dicarboxylate (**22**) 3,5–bis((1–hydroxy–3,6,9,12–tetraoxatetracosan–24–yl)carbamoyl)benzoic acid **13** (0.100 g, 1.08 mmol) and the reduced, proline functionalized spacer **20** (55.9 mg, 1.19 mmol, 1.1 eq.) were dissolved in 1 ml DMF. DMT–MM (70 mg, 0.253 mmol, 2.4 eq.) was added and the mixture was stirred at room temperature overnight. 5 ml chloroform was added and the solution was transferred to a separatory funnel. The organic layer was washed with water (2x 5 ml) and brine (5 ml) and dried over $MgSO_4$. The solvent was removed *in vacuo* and the crude was purified by reverse phase column chromatography (acetonitrile/water/tetrahydrofuran 67/33/0 to 60/20/20 v/v/v). Yield = 51.8 mg (34.8%). The coupling of **20 B** to the BTA yields a ~20% impurity (based on LCMS) as shown below.

^{1}H NMR (400 MHz, $CDCl_3$): δ = 8.36 (m, 3H, Ar), 6.72–6.54 (m, 3H, C=ONHCH$_2$), 5.25 (bs, 1H, C=OOCH), 4.25 (m, 1H, CH$_2$CHC=O), 3.75–3.54 (m, 34H, O-(CH$_2$)$_2$-O), CHCH$_2$N, 3.51–3.38 (m, 10H, CH$_2$CH$_2$NHC=O, CH$_2$CH$_2$CH$_2$O), 2.78 (bs, 2H, CH$_2$OH), 2.40–2.25 (m, 3H, CH$_2$CH$_2$C=O, CHCH$_2$CH), 2.21–2.10 (m, 1H, CHCH$_2$CH), 1.74–1.51 (m, 10H, CH$_2$CH$_2$CH$_2$O, CH$_2$CH$_2$CH$_2$O, CH$_2$CH$_2$C=O), 1.49–1.41 (m, 18H, CCH$_3$), 1.41–1.20 (m, 46H, aliphatic). ^{13}C NMR (100 MHz, $CDCl_3$) δ = 165.69, 135.27, 110.01, 77.33, 77.33, 77.01, 77.01, 76.69, 76.69, 72.54, 72.54, 71.55, 70.62, 70.62, 70.56, 70.56, 70.33, 70.33, 70.02, 61.72, 51.98, 40.37, 29.55, 29.55, 29.49, 29.44, 29.39, 29.20, 29.03, 28.38, 28.33, 28.02, 27.94, 26.92, 26.03, 26.03. LCMS: calcd. $[M + Na]^+$ 1403.94, found 1404.08. FT–IR (ATR) ν (cm^{-1}): 3335, 3074, 2926, 2855, 1740, 1706, 1649, 1537, 1458, 1399, 1367, 1288, 1259, 1149, 1125, 942, 842, 772, 707, 555.

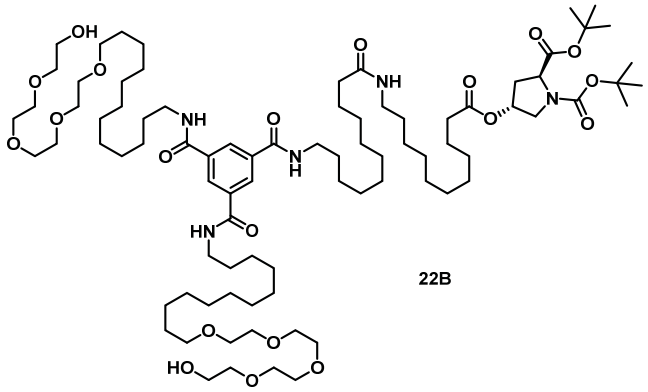

LCMS: calcd. [**22 B** + Na]$^+$ 1587.10, found 1587.17.

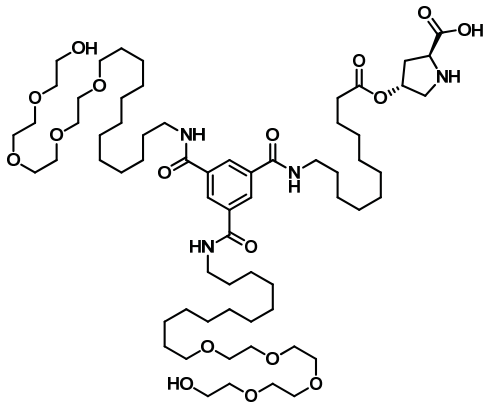

(*2S,4R)–4–((11–(3,5–bis((1–hydroxy–3,6,9,12–tetraoxatetracosan–24 yl)carbamoyl)benzamido)undecanoyl)oxy)pyrrolidine–2–carboxylic acid* (**2**) The functionalized BTA **22** (293 mg, 0.212 mmol) was dissolved in 4 ml 1:1 dichloromethane:trifluoroacetic acid and stirred overnight at room temperature. The volatiles were removed under a nitrogen stream, 2 ml of water was added and the solution was stirred overnight. The water was removed on the freeze dryer and the crude was purified by reverse phase column chromatography (water/acetonitrile 50/50 to 30/70 v/v) yielding the title compound as a sticky, white solid (182 mg, 70%)

^{1}H NMR (400 MHz, $CDCl_3$): δ = 8.39 (m, 3H, Ar), 7.61 (bs, 1H, C=ON<u>H</u>CH_2), 7.49 (bs, 2H, C=ON<u>H</u>CH_2), 5.34 (bs, 1H, C=OOC<u>H</u>), 5.13 (m, 1H, CH_2C<u>H</u>COOH), 4.36 (m, 2H, CHC<u>H_2</u>NH), 3.76–3.53 (m, 32H, O-$(CH_2)_2$-O), 3.49–3.28 (m, 10H, CH_2C<u>H_2</u>NHC=O, CH_2CH_2C<u>H_2</u>O), 2.50–2.24 (m, 4H, CH_2C<u>H_2</u>C=O, CHC<u>H_2</u>CH), 1.65–1.41 (m, 10H, CH_2C<u>H_2</u>CH_2O, C<u>H_2</u>CH_2CH_2O, C<u>H_2</u>CH_2C=O), 1.39–1.18 (m, 46H, aliphatic). ^{13}C NMR (100 MHz, $CDCl_3$) δ = 172.99, 166.72, 134.94, 128.70, 75.60, 72.42, 71.51, 70.29, 70.43, 70.03, 69.82, 61.37, 40.48, 33.81, 29.47, 29.40, 29.35, 29.24, 28.99, 28.79, 28.70, 26.97, 26.78, 25.95, 24.45. LCMS: calcd. $[M+H]^+$ 1225.83, found 1226.17. FT–IR (ATR) ν (cm^{-1}): 3320, 3073, 2925, 2855, 1740, 1648, 1545, 1456, 1349, 1290, 1200, 1131, 940, 831, 799, 720.

2.5. References

(1) Leenders, C. M. A.; Albertazzi, L.; Mes, T.; Koenigs, M. M. E.; Palmans, A. R. A.; Meijer, E. W. *Chem. Commun.* **2013**, *49*, 1963–1965.

(2) Sakthivel, K.; Notz, W.; Bui, T.; Barbas, C. F. *J. Am. Chem. Soc.* **2001**, *123*, 5260–5267.

(3) Mase, N.; Nakai, Y.; Ohara, N.; Yoda, H.; Takabe, K.; Tanaka, F.; Barbas, C. F. *J. Am. Chem. Soc.* **2006**, *128*, 734–735.

(4) Mase, N.; Barbas, III, C. F. *Org. Biomol. Chem.* **2010**, *8*, 4043–4050.

(5) Giacalone, F.; Gruttadauria, M.; Agrigento, P.; Noto, R. *Chem. Soc. Rev.* **2012**, *41*, 2406–2447.

(6) Sawada, Y.; Matsumoto, K.; Katsuki, T. *Angew. Chem. Int. Ed.* **2007**, *46*, 4559–4561.

(7) Kemme, S. T.; Šmejkal, T.; Breit, B. *Adv. Synth. Catal.* **2008**, *350*, 989–994.

(8) Lin, F. L.; Hoyt, H. M.; van Halbeek, H.; Bergman, R. G.; Bertozzi, C. R. *J. Am. Chem. Soc.* **2005**, *127*, 2686–2695.

(9) Valeur, E.; Bradley, M. *Chem. Soc. Rev.* **2009**, *38*, 606–631.

(10) Coste, J.; Le-Nguyen, D.; Castro, B. *Tetrahedron Lett.* **1990**, *31*, 205–208.

(11) Wuts, P. G. M.; Greene, T. W. *Protective groups in organic synthesis*; 4th ed.; Wiley-Interscience: Hoboken, N.J., 2007.

(12) West, K. R.; Bake, K. D.; Otto, S. *Org. Lett.* **2005**, *7*, 2615–2618.

(13) Neises, B.; Steglich, W. *Angew. Chem. Int. Ed. Engl.* **1978**, *17*, 522–524.
(14) Moore, J. S.; Stupp, S. I. *Macromolecules* **1990**, *23*, 65–70.
(15) Montalbetti, C. A. G. N.; Falque, V. *Tetrahedron* **2005**, *61*, 10827–10852.
(16) Kunishima, M.; Kawachi, C.; Monta, J.; Terao, K.; Iwasaki, F.; Tani, S. *Tetrahedron* **1999**, *55*, 13159–13170.
(17) Kamiński, Z. J.; Paneth, P.; Rudziński, J. *J. Org. Chem.* **1998**, *63*, 4248–4255.

Chapter 3 Characterizing the self-assembly behavior of *L*-proline functionalized benzene-1,3,5-tricarboxamides

3.1. Introduction

In the previous chapter, we described the synthesis of the two *L*-proline functionalized BTA derivatives **1** and **2** (Figure 3.1). In this chapter, we discuss the self-assembly of these compounds in detail to explore the influence of the structural changes. Various techniques are used to characterization the system, including infrared spectroscopy (IR), UV-Vis spectroscopy, circular dichroism (CD) spectroscopy, dynamic light scattering (DLS), small-angle X-ray scattering (SAXS), and cryogenic transmission electron microscopy (cryo-TEM).

Ideally, self-assembly of **1** and **2** in aqueous solutions results in supramolecular fibers, having a hydrophobic core around the catalytic *L*-proline, allowing it to be a more active and selective catalyst.[1] In order to explore the extent to which these highly ordered supramolecular fibers are formed, the previously mentioned techniques will be used. Self-assembly of **3** into long, one-dimensional fibers was already shown previously.[2] Apart from self-assembly, we also aim to show co-assembly of **1** and **2** with **3**, which is important to dilute the local *L*-proline concentration in the stacks and test our hypothesis that proline moieties are more active if they are present in close proximity.

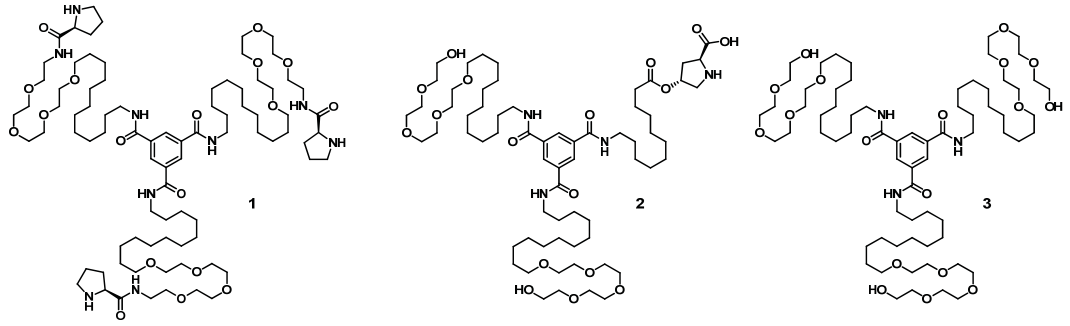

Figure 3.1: Chemical structures of water soluble, *L*-proline functionalized BTAs 1 and 2 as well as the unfunctionalized BTA 3.

3.2. BTAs in the solid state – Infrared spectroscopy

Infrared spectroscopy (IR) was used to evaluate the presence of intermolecular hydrogen bonding in the solid state. The influences of the introduced substitutions on the packing of the BTA moieties in the bulk will become visible as a shift in the position of the hydrogen bonding peaks.

Vibrations around 3240 cm^{-1} for the N-H stretch peak were shown to be indicative for the presence of threefold intermolecular hydrogen bonding of BTAs in the solid state.[3] Interpretation of this region is more complicated for **1** and **2** due to the presence of additional peaks, caused by vibrations of the amine functionality of **1** as well as the acid- and alcohol functionality of **2**. Nevertheless, both **1** and **3**

show vibrations around 3240 cm^{-1}, suggesting the presence of hydrogen bonding (Figure 3.2), while for **2**, the NH-stretch peak is shifted to 3314 cm^{-1}, suggesting non-hydrogen bound amides.

The absorption wavelength of the C=O stretch peak and the amide II vibration band can give additional information about the presence of hydrogen bonding in the solid state. For **3**, the position of the C=O stretch peak at 1641 cm^{-1} as well as the amide II vibration band at 1562 cm^{-1} are in agreement with the values reported for a threefold intermolecular hydrogen bonded structure.[3] For **1**, the spectrum is more complicated due to the presence of three additional amides on the periphery which are able to form hydrogen bonds as well. As a result, the spectrum contains overlapping peaks in the region around 1650 cm^{-1}, an area crucial to determine the presence of hydrogen bonding *via* shift of the C=O stretch peak. For **2**, additional peaks arise in the region 1750 cm^{-1} to 1550 cm^{-1}, caused by the C=O stretch of the ester and carboxylic acid functionality of the *L*-proline. Due to the overlap of those peaks with the C=O stretch peak and amide II vibration band at the BTA core, the structure formed in the solid stated cannot be determined. Overall, based on IR, **3** seems to form a threefold intermolecular hydrogen bonded structure whereas no conclusive prove about the packing of **1** and **2** in the solid state can be given.

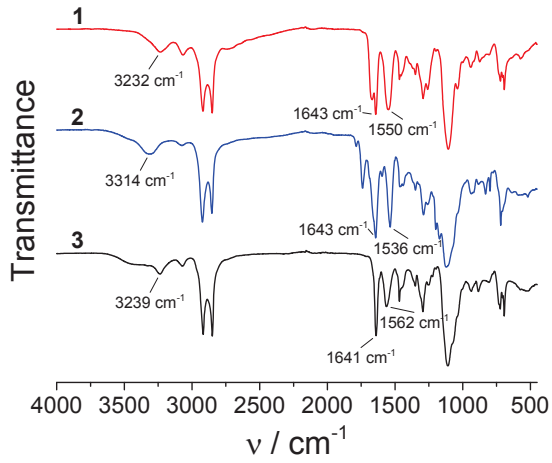

Figure 3.2: FT-IR spectra of 1 (top), 2 (middle) and 3 (bottom).

3.3. Self-assembly of BTAs in dilute solution

3.3.1. UV-Vis spectroscopy

Evaluation of the UV-Vis spectra of dilute aqueous solutions of **1** and **2** in water allows us to study the solution phase aggregation behavior of **1** and **2.** Previously, Leenders *et al*. studied the self-assembly of **3** and observed a UV-Vis spectrum for the aggregated state with two distinct absorption bands at 211 nm and 226 nm, whereas the single band at 209 nm at elevated temperatures is indicative for aggregate disruption (Figure 3.3).[2]

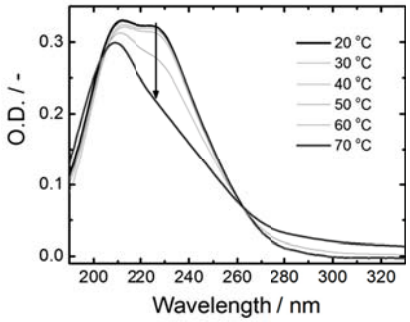

Figure 3.3 UV-Vis absorption of 3 (c = 1 x 10^{-5} M) in water, as a function of temperature (the arrow indicates the trend upon heating). Figure reprinted from reference [2].

The *L*-proline moieties of BTA derivatives **1** and **2** are charged in pure water (*trans*-4-hydroxyproline: pK_a (carboxyl) = 1.95, pK_a (amino) = 9.47),[4] and the resulting electrostatic repulsion between the molecules may hamper the self-assembly. To probe whether shielding of the charges by addition of salt has an influence on the formed structures, the UV-Vis absorption was measured in both pure water and phosphate buffered saline (PBS) (pH = 7.4). In methanol, both **1** and **2** are molecularly dissolved, derived from the absorption maximum at 207 nm (Figure 3.4).[5]

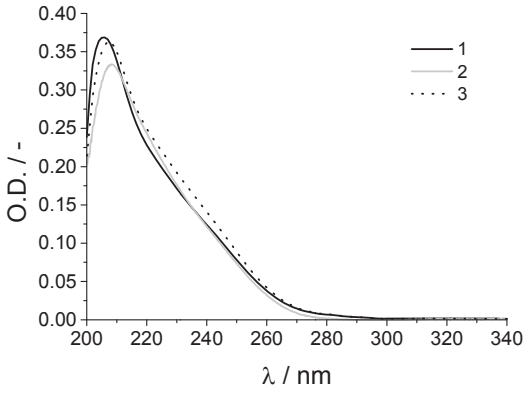

Figure 3.4: UV-Vis absorption spectra of 1, 2 and 3 in MeOH (c = 1*10^{-5} M) indicating the molecular dissolved state for all molecules.

In Figure 3.5, the UV-Vis absorption of both **1** (top) and **2** (bottom) is depicted in PBS buffer (left) and pure water (right). For each of those four systems, the ratio between functionalized BTAs **1** or **2** and unfunctionalized **3** is varied, to evaluate whether the varying degree of functionalization has an effect on the UV-Vis absorption. Comparison of the functionalized aggregates to aggregates formed by **3** was done by comparison of the graphs in Figure 3.5 to the reported UV-Vis absorption of **3** (Figure 3.3).

Most graphs in Figure 3.5, show a similar UV-Vis absorption curve as has been reported for **3** previously, thereby implying formation of the same type of aggregates. Only **1** in the absence of **3** (Figure 3.5, A and B, dotted line) shows a different curve, which is very similar to the spectrum in

methanol and seems to have a maximum at λ = 204 nm instead of the peak at 211 nm and shoulder at 226 nm. However, the observed maximum at λ = 204 nm is close to the cut-off wavelength of water and PBS (190 nm and 200 nm respectively). Since the solvent absorbs significantly in this region, the signal intensity is low and thus the signal is less reliable. Therefore, the peak at λ = 204 nm can be a measuring artifact and the actual position of the absorption peak might be at a slightly different wavelength. Nevertheless, all the other UV-Vis absorption curves in Figure 3.5 are clearly different from the curve of the molecular dissolved species (Figure 3.4), which is a clear indication that aggregates are formed in those samples.

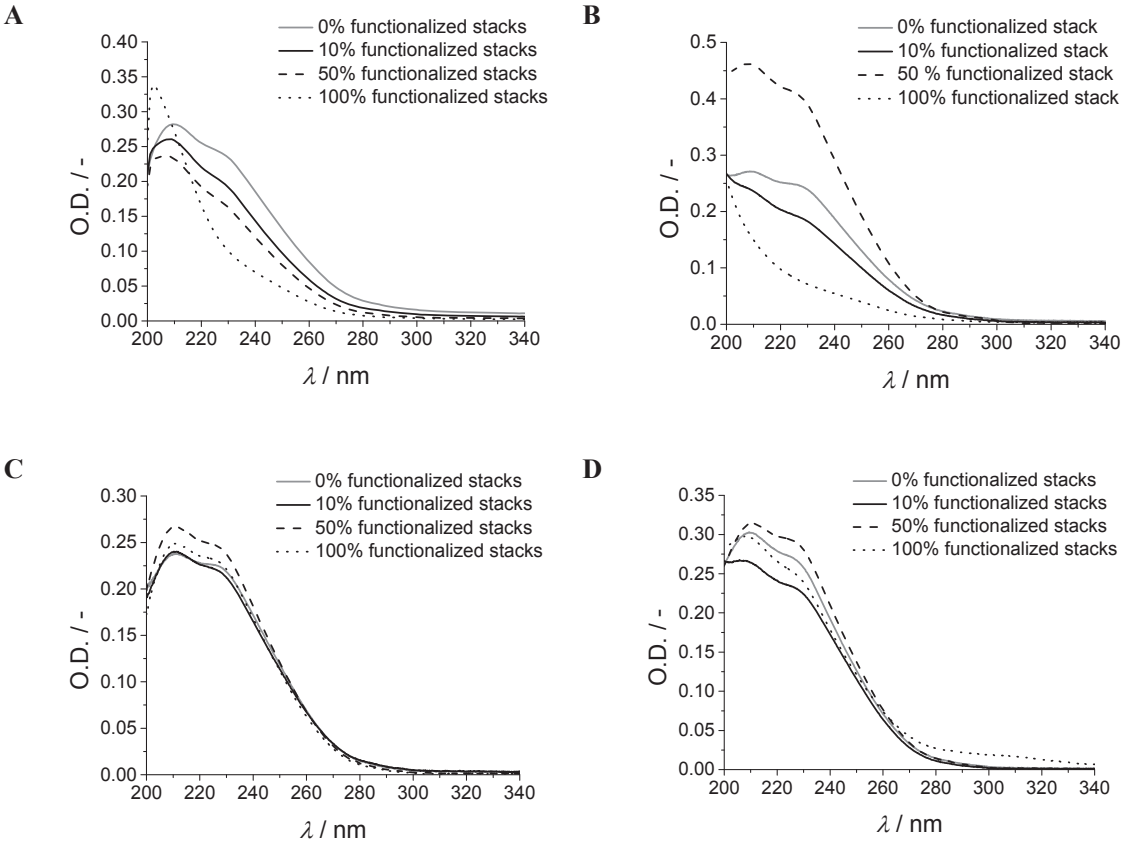

Figure 3.5: UV-Vis absorption spectra (c = 1*10^{-5} M). A: BTA 1 in PBS buffer. B: BTA 1 in water. C: BTA 2 in PBS buffer. D: BTA 2 in water.

All spectra depicted in Figure 3.5 were measured several times with different samples. Nevertheless, no consistent spectra could be obtained for **1** in water as becomes clear from Figure 3.5 B, where large variations in the total absorption intensity can been seen. Furthermore, also in the other graphs, the intensity of the absorption maxima seems to vary slightly. Since no trend in the variations in absorption intensity in Figure 3.5 B, C, and D can be observed, these fluctuations are likely the result of small concentration fluctuations. Although the stock solutions were shown to have the correct concentration, still differences between the various samples do occur.

Although no trend of the fluctuations in absorption intensity in Figure 3.5 B, C and D was observed, this does not hold for Figure 3.5 A. In Figure 3.5 A, there is a clear trend and the curves for the 10% and 50% functionalized stacks for **1** in PBS look somewhat similar to linear combinations of curves for the 0% and 100% functionalized stacks (Figure 3.5 A). This gives rise to the possibility that **1** and **3** form separate stacks in solution. However, it is impossible to conclude from the UV-Vis data whether this is indeed the case or whether the two different BTAs do coassemble.

Comparison of the spectra measured in PBS buffer (Figure 3.5 A and C) with the spectra measured in pure water (Figure 3.5 B and D) does not reveal any significant differences, apart from the already discussed differences in absorption intensities. Since a system in pure water is simpler, due to the absence of salts that might influence the behavior of the system, we decided to perform all remaining characterizations using pure water as solvent.

3.3.2. Circular dichroism spectroscopy

An excellent method to study the self-assembly of molecules bearing a stereogenic center is circular dichroism (CD) spectroscopy. In self-assembled systems, a Cotton effect indicates the presence of chirally biased architectures. In BTAs, by introduction of a stereogenic center into the alkyl side chain close to the BTA core results in preference of one helical conformation over the other, giving rise to a distinct Cotton effect.[2,6] In this section, we explore whether the chirality from the *L*-proline in **1** and **2** is transferred to the stacks, resulting in a bias of the chirality of the stacks.

In BTA **1**, no Cotton effect is observed. Apparently, the chiral centers of the *L*-proline moieties are too far away from the BTA core to transfer their chiral information to the self-assembling unit. Even after a temperature treatment where the sample was heated to 80 °C and subsequently cooled to room temperature with 20 °C $hour^{-1}$ in order to allow the BTAs to form the thermodynamically most stable aggregates, no Cotton effect was observed.

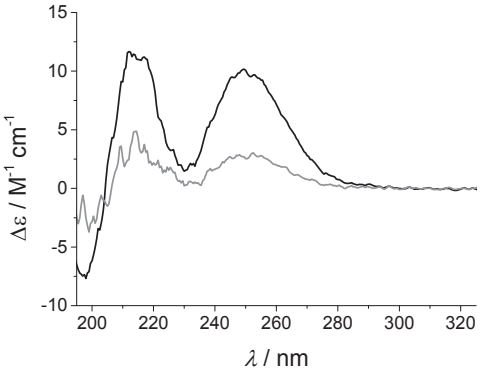

Figure 3.6: CD spectra of 2 (c = 5 x 10^{-5} M) (black) and mixed with hydroxy BTA (1:1; c_{total} = 5 x 10^{-5} M) (grey).

On the contrary, solutions of BTA **2** show a clear Cotton effect (Figure 3.6), indicating the presence of defined chiral architectures formed by self-assembly of **2** into three-dimensionally

ordered structures. Interestingly, chirality transfer occurs from the chiral *L*-proline to the BTA core, although the *L*-proline is 11 carbon atoms away from this core in the molecular structure. The Cotton effect depicted in Figure 3.6 clearly differs from the Cotton effect reported previously for a chiral derivative of **3**, thereby indicating that the supramolecular aggregates in this system differ from the reported system.[2]

Upon introduction of non-chiral BTAs to a chiral system, amplification of chirality was previously observed according to the 'sergeants-and-soldiers' principle.[6] Upon co-assembly of the chiral sergeants with the non-chiral soldiers, the sergeants strongly amplify the helical sense preference of the mixed stacks. In our system, however, no chiral amplification is observed (Figure 3.6). The intensity of the Cotton effect of the mixture of **2** with **3** is roughly half the intensity compared to the sample with **2**, for a similar total BTA concentration. The absence of chiral amplification can be explained by either the inability of **2** to behave as a sergeant or by assembly of the molecules into separate stacks. Therefore, this experiment neither confirms nor excludes coaggregation of the two BTAs.

3.4. Characterization of aggregate size and shape

3.4.1. Dynamic light scattering

Dynamic light scattering experiments (DLS) were used to assess the diffusion coefficient of the aggregates. Since the diffusion coefficient is related to the aggregate size, DLS may yield more information about the differences between the aggregates formed by **1** and **2**.

In a DLS experiment the sample is irradiated with a monochromatic light beam and the intensity of the scattered beam is recorded. The positions of particles in the sample change due to Brownian motion resulting in fluctuations in the overall scattering intensity. These fluctuations are related to the particle's diffusion coefficients: the fast diffusion of small particles results in a rapid fluctuation of the intensity whereas the opposite is true for large particles (Figure 3.7). Comparison of the intensity of signal at time = t to the intensity at time = t + τ where τ is the delay time yields the correlation function G(τ). The fast change in scattering intensity of small particles results in a fast decay of the correlation function, whereas the opposite is true for large particles.

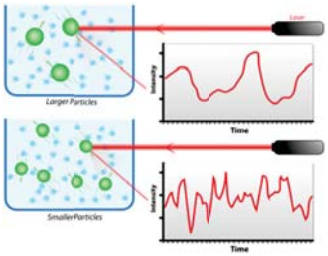

Figure 3.7: Typical fluctuations in scattered intensity for large particles (top) and small particles (bottom).[7]

DLS measurements were kindly performed by Gijs ter Huurne on both BTAs **1** and **2** as well as on mixtures of **1** and **2** with **3** in a 1:1 ratio. The decay times of the correlation functions of the different samples are very similar (Figure 3.8), suggesting comparable diffusion rates. The size of the aggregates could not be determined from these DLS measurements due the high polydispersity of the sample. However, the raw data revealed a lower count rate for samples containing **1** than for samples containing **2** (Figure 3.8, inset), suggesting the presence of less scattering centers and thus less aggregation in **1**.

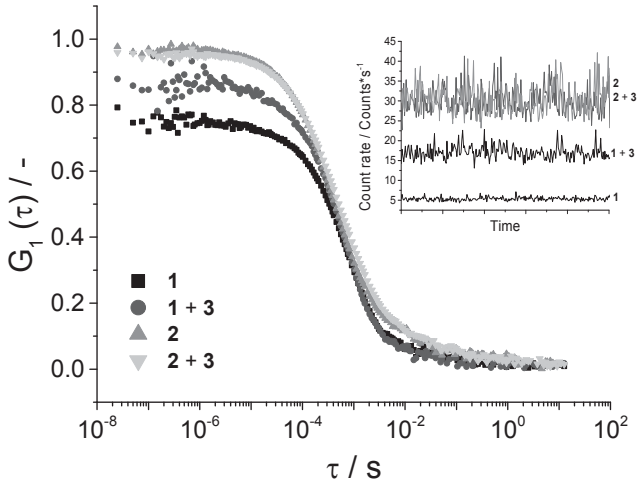

Figure 3.8: DLS measurement revealing similarly sized aggregates for mixtures of both BTA 1 and 2 with 3 (c_{total} = 0.45 mg/ml, ϑ = 90°, room temperature). The inset shows the count rate of the raw data.

Multi-angle DLS measurements were done to obtain information about the shape of the aggregates. Unfortunately, the polydispersity of the samples was found to be too high to obtain any valuable data from these experiments.

3.4.1. Small-angle X-ray scattering

Small-angle X-ray scattering (SAXS) was used to access additional information about the structure of the aggregates that are formed upon self-assembly of **1** and **2**. The principles of SAXS are somewhat similar to DLS. However, due to the use of more energetic X-rays, SAXS measurements allow access to smaller length scales. Furthermore, the information for SAXS is extracted from the form factor, which is based on the average value of the scattered light instead of the fluctuations. The form factor contains information about shape and size of the particles (Figure 3.9).[8] The slope of the form factor at small scattering angles yields information about the overall size of the aggregates, where a power law of 0, -1 or -2 corresponds to a globular, cylindrical and lamellar shape, respectively. If the form factor is fitted with mathematical models, quantitative information about the particle's dimensions can be extracted.

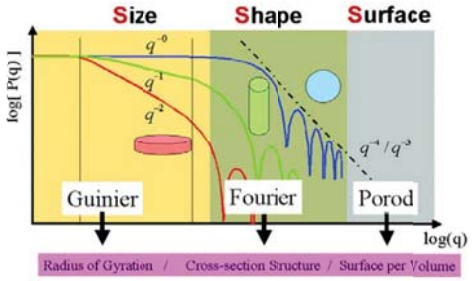

Figure 3.9: The scattering curves for simple particle shapes and its basic information domains.[8]

SAXS experiments were kindly performed by Ilja Voets. The SAXS data of **1** (Figure 3.10 A) shows a power law of 0 in the low q-range being characteristic for small, sphere-like objects with an aspect ratio close to unity. In contrary to **1**, the SAXS profiles of **2** (Figure 3.10 B) show clear q^{-1} behavior, indicative for the presence of long cylinders. The uncommon decay of the data of **1** at low q values is caused by ordering of the aggregates, caused by electrostatic repulsion between the molecules.

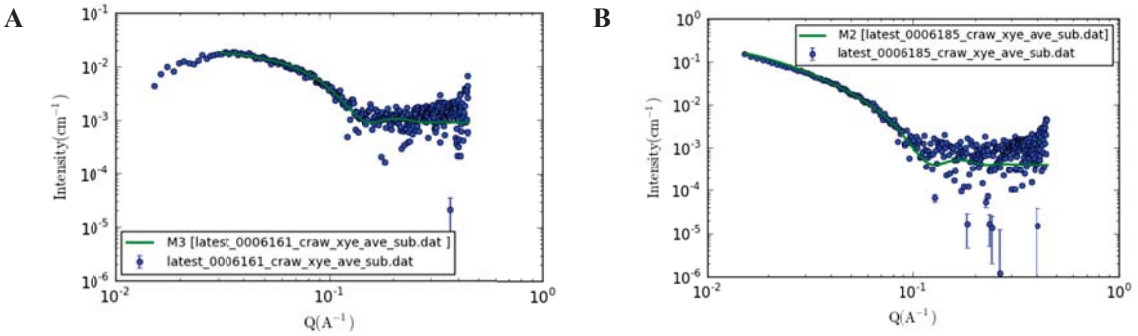

Figure 3.10: Experimental small angle X-ray scattering profiles of proline BTAs (25 °C, c = 0.45 mg ml^{-1}). Solid lines are fits with a form factor model for flexible cylinders (i.e., the Schurtenberger-Pedersen form factor for worm-like, self-avoiding chains).

The data obtained for the two BTAs can be fitted to a worm-like chain model, which assumes an isotropic, continuously flexible rod. However, the results of the fitting procedure have to be interpreted carefully, because the SAXS data contains a lot of noise especially in the high q-regime. The fit yields values for the length of the polymer, L, the Kuhn length, L_K, and the cross-sectional radius r_{cs}. The Kuhn length is a measure for the stiffness of the polymer, where higher values for L_K correspond to a stiffer polymer.

The data obtained for **1** can be fitted to both a model for spheres as well as to the worm-like chain model, because SAXS cannot distinguish between small spheres and short stacks on these length scales. Data analysis with the worm-like chain model at 25 °C yields L ~ 33 nm, L_K ~ 4.1 nm, and a r_{cs} of 2.4 nm. For **2**, we find L ~ 70 nm, L_K ~ 5.0 nm, and a r_{cs} of 3.0 nm, suggesting the presence of high aspect ratio fibers with a length of more than 70 nm (the limit of the spectral window). Based on

these data, we can conclude that **1** forms either short stacks or sphere-like aggregates whereas **2** forms long cylinders.

3.4.2. Cryogenic transmission electron microscopy

In order to visualize the formed aggregates, cryogenic transmission electron microscopy (cryo-TEM) can be used. Cryo-TEM is very suitable to study the molecular structure of BTAs in aqueous solution, since, in contrast to common transmission electron microscopy, drying of the sample and fixation to a grid is not necessary. The sample is frozen in a thin layer of amorphous ice instead, thereby avoiding deformation and collapse of the sample.[9] As a result, the sample can be investigated in a frozen hydrated state in which the molecular structure is preserved.

A disadvantage of cryo-TEM, however, is the time consuming sample preparation and measuring. Furthermore, the absence of aggregates in a cryo-TEM image does not yield any information about the sample, since aggregates may be present that cannot be visualized because they are frozen in a too thick layer of ice or they lack contrast, for example.

Cryo-TEM was kindly measured by René Lafleur of samples with a total BTA concentration of 0.5 mg ml^{-1}. Upon visual inspection of these samples, we noticed a significantly increased viscosity, which is an indication for the formation of aggregates by both **1** and **2**. However, for **1**, no aggregates could be observed in the sample. As briefly discussed previously, this might have a number of reasons, but does not give any information about the presence of aggregates.

The aggregates in a sample of **2** were successfully visualized by cryo-TEM. Long, one-dimensional, fiber-like structures formed by self-assembly of **2** can be clearly seen in Figure 3.11. The dark spherical objects in the images are typical ice crystals and thus do not correspond to aggregated BTAs. Unfortunately, it is not possible to extract a number for the length of the aggregates from the pictures, but the image suggests aggregates with lengths in the micrometer range. Due to the relative poor contrast of these images, the diameter can be estimated only roughly to be <10 nm.

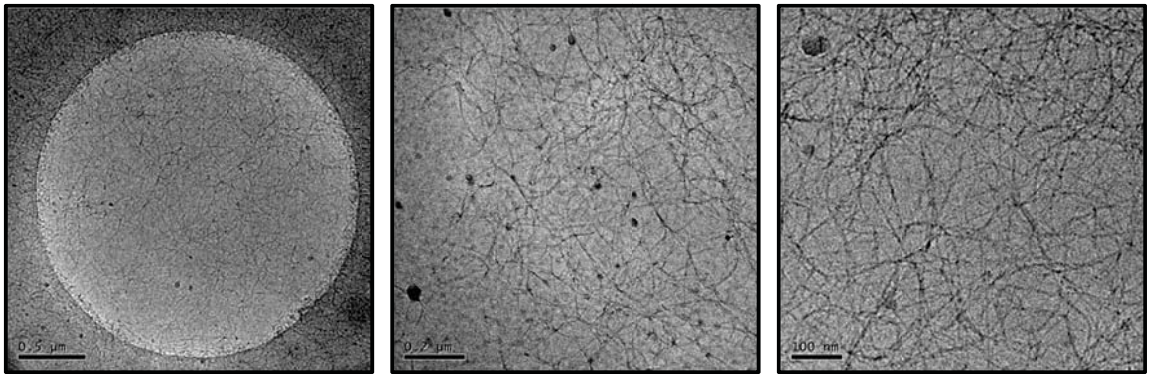

A **B** **C**

Figure 3.11: Cryo-TEM images of BTA 2 at different magnifications clearly showing the presence of high aspect ratio fibers (c = 0.5 mg/mL).

3.5. Conclusions

The aggregation of *L*-proline functionalized BTAs **1** and **2** was evaluated using various techniques. Self-assembly of BTA **1** in aqueous solution was shown to yield either short stacks or spheres. The different UV-Vis absorption of **1** compared to **3** and mixtures of **1** and **3**, suggests self-assembly of **1** into different aggregates. The formation of aggregates is confirmed by SAXS, where data characteristic for spherical objects with an aspect ratio close to unity were obtained. A possible explanation of these results is the formation of small stacks or spheres upon self-assembly of **1** that do not grow beyond a certain size due to the electrostatic repulsion between charged *L*-proline moieties.

BTA **2** was shown to self-assemble into one-dimensional stacks. UV-Vis spectroscopy of **2** as well as mixtures of **2** and **3** yields an absorption spectrum analogous to the spectra reported for **3**, suggesting the formation similar aggregates. Furthermore, although DLS experiments yielded comparable diffusion rates for **1** and **3**, more aggregation seems to be present in samples of **2** compared to **1**. SAXS data of **2** showed the formation of cylinders with a high aspect ratio and ultimately one-dimensional stacks could be visualized using cryo-TEM.

3.6. Experimental section

3.6.1. Materials

All reagents were purchased from Aldrich, Acros Organics or Fluka and used as received, unless otherwise specified. HPLC grade solvents were purchased from Scarlab, Biosolve and/or Carlo Erba and use without further purification. All other solvents were purchased from Biosolve. Milli-Q water was purified on an EMD Millipore Milli-Q Integral Water Purification System.

3.6.2. Methods

Infrared spectroscopy

IR spectra were recorded on a Perkin Elmer Spectrum 2 FT-IR spectrometer equipped with a universal ATR sampling accessory for solid samples.

UV-Vis spectroscopy

UV-Vis experiments were performed on a Jasco V-650 spectrophotometer equipped with a JASCO ETCR-762 temperature controller or a Varian 300 Bio UV-Visible spectrophotometer equipped with a Varian Carey temperature controller. UV-Vis absorption experiments were performed with a scan speed of 40 nm / min, a data pitch of 0.5 nm, a bandwidth of 1.0 nm, spanning the wavelength range of 190 nm or 200 nm (water and PBS buffer respectively) to 340 nm. A quartz cuvette with 1 cm path length was used for all measurements.

Sample preparation: Injection method

Stock solutions were prepared by dissolving the correct amount of resp. hydroxy BTA, BTA **1** and BTA **2** in methanol to create solutions with a total concentration of 10 mM. Subsequently, these solutions were mixed in the correct ratios yielding stock solutions with 0%, 10%, 50% and 100% functionalized BTAs. 3.5µL of these stock solutions was injected into 3.5 ml demineralized water or

Phosphate buffered saline (PBS), to give a total BTA concentration of $1*10^{-5}$ M. The samples were annealed overnight and measured afterwards.

Circular dichroism spectroscopy

Circular dichroism measurements were performed with a Jasco J-815 spectro polarimeter in combination with a PFD-425S/15 Peltier-type temperature controller. For all experiments the linear dichroism (LD) was also measured and in all cases no LD was observed. The molar circular dichroism $\Delta\varepsilon$ was calculated from $\Delta\varepsilon$ = CD effect / (32980 · c · l) in which c is the concentration and l is the optical pathway. Typical CD measurements were performed at a concentration of 5×10^{-5} M and an optical pathway of 1 cm. The injection method was used for the sample preparation. However, stock solutions with a concentration of 15 mM were prepared of which 10 µL was added to 3 mL water.

Small angle X-ray scattering

Small angle X-ray scattering measurements were performed by Ilja Voets on a SAXSLAB GANESHA 300 XL SAXS system equipped with a GeniX 3D Cu Ultra Low Divergence micro focus sealed tube source producing X-rays with a wavelength λ = 1.54 Å at a flux of $1x10^8$ ph/s and a Pilatus 300K silicon pixel detector with 487 x 619 pixels of 172 μm^2 in size placed at a sample-to-detector distances of 713 to access a q-range of $0.15 \leq q \leq 4.39$ nm^{-1} with $q = 4\pi/\lambda(\sin\vartheta/2)$. Silver behenate was used for calibration of the beam centre and the q range. Samples were contained in 2 mm quartz capillaries (Hilgenberg Gmbh, Germany).

The two-dimensional SAXS patterns were brought to an absolute intensity scale using the calibrated detector response function, known sample-to-detector distance, measured incident and transmitted beam intensities, and azimuthally averaged to obtain one-dimensional SAXS profiles. The scattering curves of the supramolecular polymers were obtained by subtraction of the scattering contribution of the solvent and quartz cell.

Sample preparation: Dry mix method

Stock solutions of the functionalized BTA **1** and **2** in MeOH were prepared. 0.45 mg of compound was put into a vial and the solvent was removed under a stream of argon and subsequently in the vacuum oven at 40°C yielding the compounds as a solid. Afterwards, 0.5 ml milli-Q water was added and the sample was sonicated during two minutes yielding a slightly turbid solution. After equilibration over night at room temperature, a completely clear solution was obtained.

Data analysis:

The small angle X-ray scattering profiles were analyzed using the software package SasView (http://www.sasview.org/). We selected a form factor developed originally for semi-flexible, self-avoiding polymer chains by Pedersen and Schurtenberger to which we refer as the worm-like chain (WLC) model and a form factor for a homogeneous sphere.[10] The former describes the scattering profiles of the supramolecular chains in terms of a contour length, L_c, a Kuhn length, L_K, and a cross-sectional radius, r_{cs}.

Dynamic light scattering

Dynamic light scatteing experiments were conducted on an ALV/CGS-3 MD-4 compact goniometer system equipped with a multiple tau digital real time correlator (ALV-7004) and a solid state laser (λ = 532 nm; 40 mW).

The dry-mix method was used for the sample preparation, however, the milli-Q water was filtered prior to use with a 0.1 µm AT-filter (Whatman) in order to prevent the presence of dust.

Cryogenic transmission electron microscopy

Cryogenic transmission electron microscopy was kindly measured by René Lafleur on samples with a concentration of 0.5 mg/mL. Samples were prepared in a 'Vitrobot' instrument (PC controlled vitrification robot, patent applied, Frederik et al 2002, patent licensed to FEI) at room temperature and a relative humidity >95%. In the preparation chamber of the 'Vitrobot' a 3µl sample was applied on a Quantifoil grid (R 2/2, Quantifoil Micro Tools GmbH; freshly glow discharged just prior to use), excess liquid was blotted away for 2 s at -2 mm and the thin film thus formed was shot (acceleration about 3 g) into liquid ethane. The vitrified film was transferred to a cryoholder (Gatan 626) and observed at -170 °C in a Tecnai Sphera microscope operating at 200 kV. Micrographs were taken at low dose conditions.

Sample preparation:

The dry-mix method was used for the sample preparation. However, the amount of sample was adjusted to yield a 0.5 mg/ml solution of BTA in water.

3.7. References

(1) Zotova, N.; Franzke, A.; Armstrong, A.; Blackmond, D. G. *J. Am. Chem. Soc.* **2007**, *129*, 15100–15101.
(2) Leenders, C. M. A.; Albertazzi, L.; Mes, T.; Koenigs, M. M. E.; Palmans, A. R. A.; Meijer, E. W. *Chem. Commun.* **2013**, *49*, 1963–1965.
(3) Cantekin, S.; de Greef, T. F. A.; Palmans, A. R. A. *Chem. Soc. Rev.* **2012**, *41*, 6125–6137.
(4) Lide, D. R. *CRC Handbook of Chemistry and Physics, 84th Edition*; CRC Press, 2003.
(5) Brunsveld, L.; Schenning, A. P. H. J.; Broeren, M. A. C.; Janssen, H. M.; Vekemans, J. A. J. M.; Meijer, E. W. *Chem. Lett.* **2000**, *29*, 292–293.
(6) Smulders, M. M. J.; Schenning, A. P. H. J.; Meijer, E. W. *J. Am. Chem. Soc.* **2008**, *130*, 606–611.
(7) http://en.wikipedia.org/wiki/Dynamic_light_scattering.
(8) Schnablegger, H.; Singh, Y. *The SAXS guide*; 2nd ed.; Anton Paar GmbH: Austria, 2011.
(9) Wang, L.; Sigworth, F. J. *Physiology* **2006**, *21*, 13–18.
(10) Pedersen, J. S.; Schurtenberger, P. *Macromolecules* **1996**, *29*, 7602–7612.

Chapter 4 Investigating the catalytic properties of *L*-proline functionalized benzene-1,3,5-tricarboxamides in water

4.1. Introduction

In this chapter, we will elaborate on the catalytic properties of the *L*-proline functionalized BTAs **1** and **2**. These BTAs are designed to show catalytic activity towards the aldol reaction in an aqueous environment. Ideally, self-assembly of **1** and **2** (Figure 4.1) in water results in highly ordered aggregates, providing a hydrophobic domain around the catalytic *L*-proline, since *L*-proline is a more active and selective catalyst in hydrophobic surroundings.[1] It was hypothesized that the molecular design of **2**, where the ethylene glycol spacer between the hydrophobic core and the *L*-proline is omitted, allows for better incorporation of *L*-proline into the hydrophobic interior of the BTA stacks, thereby resulting in a more active and selective catalyst compared to **1**.

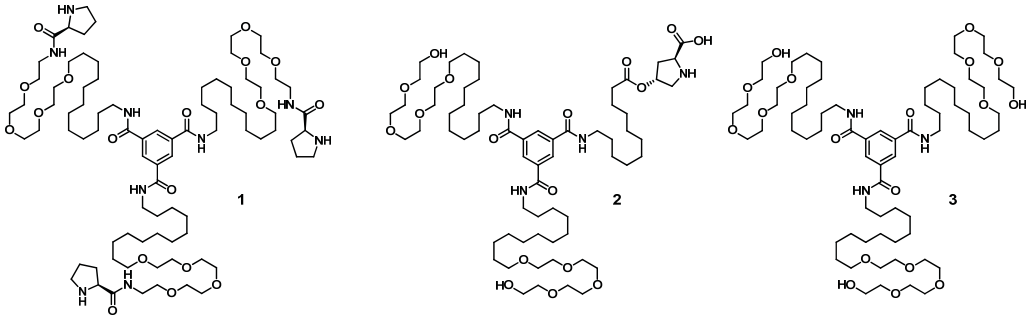

Figure 4.1: Chemical structures of water soluble, *L*-proline functionalized BTAs 1 and 2 as well as the unfunctionalized BTA 3.

The design of the system allows for tuning of the local *L*-proline density in the stacks by variation of the ratio functionalized BTA **1** or **2** to unfunctionalized BTA **3**. Thereby, we can investigate the hypothesis that the catalytic activity of *L*-proline moieties is higher if multiple moieties are present in close proximity.[2] In order to dilute the local catalyst concentration upon addition of **3**, coassembly of **1** and **2** with **3** is a prerequisite. Although, we did not prove coassembly directly (chapter 3), various different functionalized derivatives of **3** were shown to coassemble with **3** in this group previously, including dye-, peptide-, and saccharide functionalized BTAs.[3–5] Therefore, coassembly of **1** and **2** with **3** was assumed.

The idea of *L*-proline functionalized BTAs for the aldol reaction in water was already studied by Huerta *et al*. who showed single chain polymeric nanoparticles (SCPN) with *L*-proline moieties embedded in the particle's hydrophobic core to have good catalytic properties (Figure 1.10).[6] A catalyst loading of 5 mol% was shown to result in over 50% conversion within 24 hours, while high stereoselectivities were obtained (*de* = 91% and *ee* = 98%).

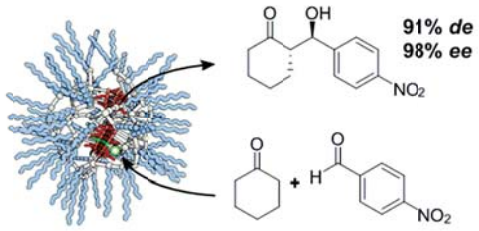

Figure 4.2: Schematic representation of the catalytically active SCPNs.[6]

By serendipity it was found that the *L*-proline functionalized BTAs (Figure 4.3 A) can be very active as well in absence of the hydrophobic core of the SCPN if they are subjected to a temperature treatment (Figure 4.3 B).[7,8] Unfortunately, characterization of this system is very cumbersome and it is still not entirely clear what causes the unexpected high catalytic performance of the BTA-*L*-proline aggregates in water. Moreover, it is impossible to gain control over the system.

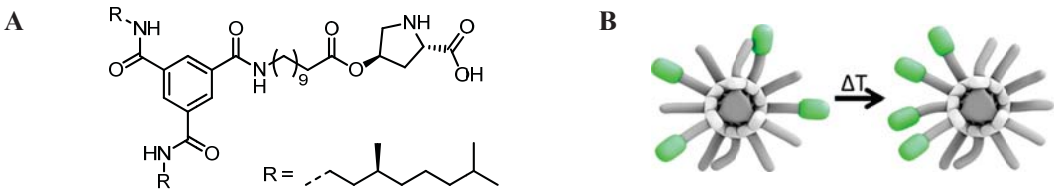

Figure 4.3: A: Molecular structure of catalytic BTA investigated by Van Genabeek. B: Proposed reorganization of the *L*-proline moieties within the BTA stack caused by the temperature treatment.[7]

In this chapter, we explore the influences of the different molecular designs of **1** and **2** on the catalytic activity and selectivity of these organocatalysts. Initial catalyst experiments performed with **1** and **2** showed unsatisfactory reproducibility and the subsequent screening of different reaction conditions will be discussed. The improved setup that was found enabled a reliable comparison of the catalytic activity of **1** and **2**, and systems reported in literature.

4.1.1. General procedure for catalysis

The catalytic activity and selectivity of **1** and **2** was evaluated using the model aldol reaction between 4-nitrobenzaldehyde and cyclohexanone. These highly reactive substrates enable a convenient analysis of the reaction products, which are directly related to catalyst activity and selectivity. Furthermore, using these frequently used substrates enables the direct comparison of our system to various systems described in literature.[9] The aldol reaction between 4-nitrobenzaldehyde and cyclohexanone can yield four stereoisomers, of which the *anti*-(*S*,*R*)-product was shown to be formed predominantly in both experimental and computational studies.[10,11]

A standard catalysis procedure was developed and used for all catalysis experiments. First, the samples were prepared following the sample preparation method described below. After equilibration overnight, the solutions were charged with substrates upon injection of a 10:1 mixture of cyclohexanone and nitrobenzaldehyde yielding a substrate concentration of 50μM. The samples were

mixed vigorously during 24 hours (unless indicated otherwise) in order to keep the water-insoluble substrates finely dispersed.

Subsequently, the products were removed from the solutions by extraction using diethyl ether. After removal of the ether under a stream of nitrogen, both conversion and diastereomeric excess (de_{anti}) were determined by ^{1}H NMR analysis. In all cases, no transfer of BTAs to the organic layer was observed, since no BTA peaks can be observed in the ^{1}H NMR spectrum. The conversion was determined by comparison of the integral at 10.16 ppm corresponding to the unreacted aldehyde with the integrals at 8.21 ppm and 7.51 ppm corresponding to the aldol product (Figure 4.4). The de_{anti} can be determined from the ratio of the product signals at 5.48 ppm (*syn*) and 4.90 ppm (*anti*) respectively as reported in literature.[12]

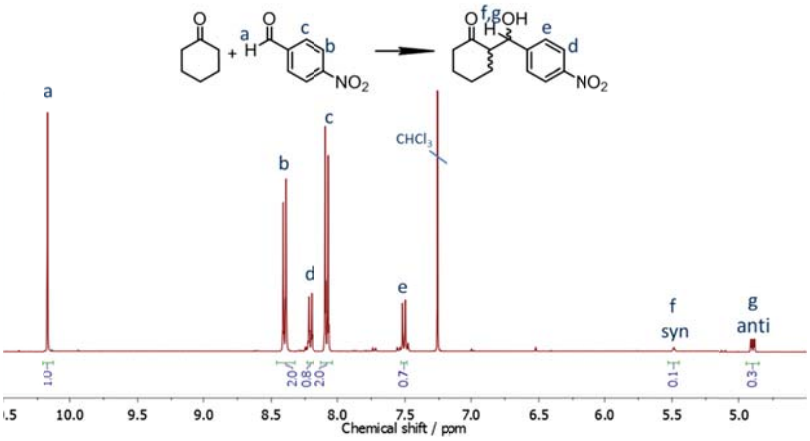

Figure 4.4: ^{1}H-NMR spectrum (400 MHz, $CDCl_3$) of the crude aldol product obtained after catalysis, showing the signals used for the determination of the conversion (27%) and *de* (65%). The aliphatic region is omitted for clarity.

The enantiomeric excess was determined by HPLC analysis using a chiral column. The value for the ee_{anti} is determined *via* integration of the peak areas corresponding to the two different *anti*-products in the HPLC profile as indicated in Figure 4.5 monitored at λ = 268 nm.

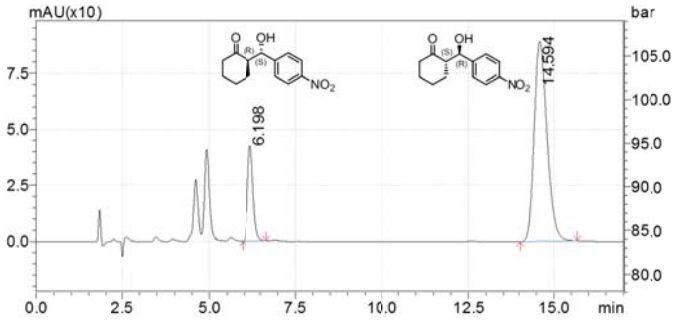

Figure 4.5: HPLC profile (λ = 268 nm) for aldol products. The peak with a retention time of 14 min belongs to the anti-enantiomer that is formed predominantly during *L*-proline catalysis whereas the peak at 6.1 min represents the minor anti-enantiomer.[6]

4.1.2. Sample preparation – Dry mix method

Generally, homogeneous samples of BTAs in water can be conveniently prepared by injection of a BTA stock solution in methanol into water. However, this method is not suitable for the preparation of samples with a high total BTA concentration, because the large volumes of methanol injected will disable the formation of supramolecular stacks. Since relatively high BTA concentrations are required in the catalysis samples, a new sample preparation method was adopted. The dry-mix method allows to prepare samples at high total BTA concentrations completely free of methanol.

For the sample preparation, separate 15 mM stock solutions of **1**, **2**, and **3** were prepared in methanol. These solutions were mixed in the correct ratio and the solvent was removed under a stream of nitrogen and subsequently in the vacuum oven at 40°C. Afterwards, water was added and the samples were sonicated for two minutes yielding slightly turbid solutions. After equilibration over night at room temperature, completely clear solutions were obtained.

In order to evaluate whether the dry mix method is a suitable sample preparation method for our system, we analyzed the UV-Vis absorption of various samples in cuvettes with an optical path length of 0.10 mm. From Figure 4.6 it becomes clear that samples containing BTA **1** (Figure 4.6 A) and **2** (Figure 4.6 B) show absorption spectra with a peak at 210 nm and shoulder at 226 nm, analogous to the spectra obtained for these compounds in dilute aqueous solution (c = 10 µM). This information suggests self-assembly of both **1** and **2** into the same aggregates as observed previously. The slightly increased baseline in the sample of BTA **2** implies the presence of scattering, which is more commonly observed for samples at these high concentrations. Furthermore, the increased viscosity of the samples that can been seen by the eye is an indication for self-assembly at these high BTA concentrations (approx. 1 mM).

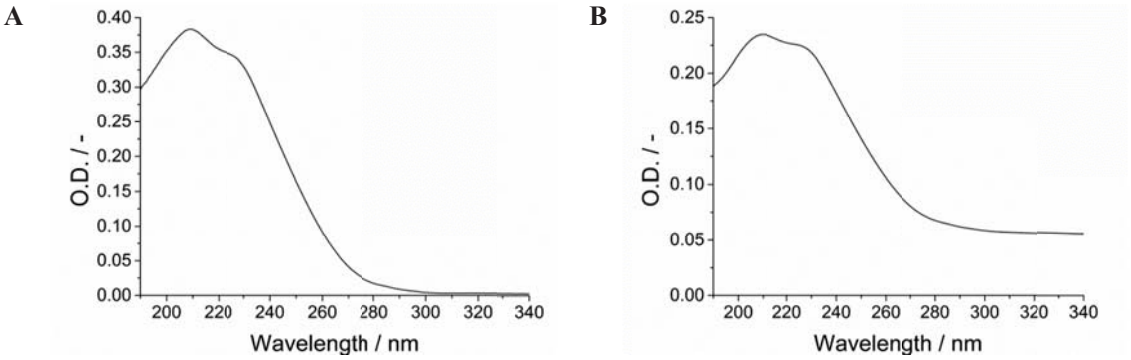

Figure 4.6: UV-Vis absorption curves of catalysis samples prepared by the dry mix method. A: 1 and 3 in a 1:1 ration (c_{total} = 1 * 10^{-3} mol L^{-1}). B: 2 and 3 in a 1:1 ratio (c_{total} = 1 * 10^{-3} mol L^{-1}).

4.2. Preliminary screening of 1

In many literature examples, *L*-proline catalyzed aldol reactions are performed at catalyst concentrations of 10 mol% to 30 mol% or even higher.[13–15] However, recently, moderate activity and good selectivity is reported for a number of proline derivatives at 1 mol% to 3 mol%.[16] Since our

symmetric *L*-proline functionalized BTA **1** may form ordered structures where the *L*-proline is shielded from the aqueous environment, we choose a challenging catalyst concentration of only 3 mol% to do the initial catalysis experiments.

The initial catalysis results with **1** showed conversions around roughly 30% and promising selectivities (de ≈ 70%, ee ≈ 68%) (Table 4.1). Because an active catalyst was obtained at a catalyst loading of 3 mol%, we kept the catalyst concentration constant and diluted the stacks with **3** to explore the influence of the local *L*-proline concentration on the catalyst activity. For example, a sample with a stack functionalization of 20% is prepared by addition of 0.27 μM **1** and 1.1 μM **3**, whereas a sample with 100% stack functionalization contains only 0.27 μM **1** (Figure 4.7).

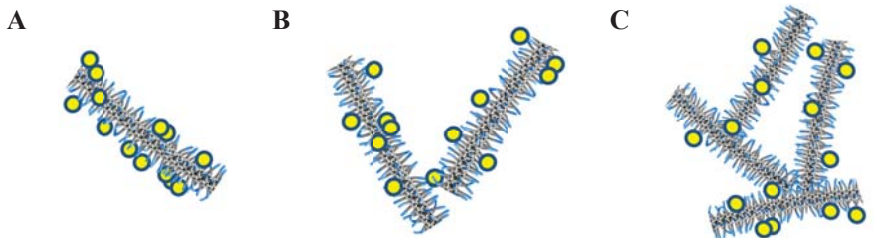

Figure 4.7: Schematic representation of halving of the stack functionalization (A to B and B to C) upon addition of unfunctionalized 3, thereby diluting the local *L*-proline concentration in the stacks.

Four different runs of samples with varying stack functionalization yielded the graph depicted in Figure 4.8. The details of four selected experiments are shown in Table 4.1. Figure 4.8 A reveals an overall trend where higher conversions are observed for stacks with a higher local *L*-proline density. Although the absolute values between different runs differ, the overall trend seem to be consistent. The reproducibility varies a lot, conversions between duplo samples differ between 2% in the best case and 25% in the worst. However, the selectivity was reasonably constant throughout the various samples (Figure 4.8 B) and thus seems to be independent of the stack functionalization.

A **B**

Figure 4.8: Conversion (A) and *de* (B) as a function of stack functionalization for catalysis with 1, suggesting higher conversion for higher local *L*-proline density.

The total BTA concentration of the selected samples in Table 4.1 is depicted in the last column of the table. Due to the experimental setup, the total BTA concentration increases upon decreasing stack density, reaching values up to almost 3 mM for the sample containing 80% **3**. At these concentrations, gel formation occurs upon equilibration of the sample. This gives rise to the question whether the lower conversions at low stack functionalizations are due to decreased activity of the catalyst or rather due to diffusion limitations. Although various proline catalyzed aldol reactions in gels have proven successful,[17] we tried to avoid this issue by lowering the catalyst concentration to 1% resulting in lower total BTA concentrations as well. However, this was unsuccessful, since conversions below 10% were obtained that could not reliably be analyzed by ^{1}H NMR due to the large error on the integrals (~5%).

Table 4.1: BTA 1 catalyzed aldol reaction for a selection of stack densities at a *L*-proline concentration of 3 mol%.

Entry	BTA	$c_{L\text{-pro}}$ (%)	Stack funct.* (%)	Conversion† (%)	de_{anti}† (%)	ee_{anti}‡ (%)	c_{BTA} (mM)
1	**1**	3	100	36	68	67	0.54
2	**1**	3	100	27	68	68	0.54
3	**1**	3	50	30	70	70	1.1
4	**1**	3	20	26	76	74	2.7

* Percentage of **1** mixed with **3**. † Determined by ^{1}H NMR. ‡ Determined by chiral HPLC. Conditions: reaction volume: 0.5 ml; aldehyde concentration: 50 mM; substrate ratio (aldehyde:ketone): 1:10; room temperature ; reaction time: 24 h.

4.3. Catalytic activity of 2

Preliminary catalysis experiments with **2** at a catalyst loading of only 1 mol% showed a promising conversion of 69%, an excellent diastereomeric excess of 96%, and enantiomeric excess of 98% (Table 4.2, entry 1). The excellent selectivities were constant throughout the experiments; however, we found the catalytic activity to be very irreproducible. In order to gain more control over our system and increase the reproducibility and activity, different sample preparation methods and reaction conditions were explored that were described in literature to yield improved catalytic behavior towards the aldol reaction of *L*-proline based catalysts in water.

4.3.1. Screening for reproducible reaction conditions

To increase the activity and reproducibility of our system, we first tested the influence of a temperature treatment as described by Bas van Genabeek[7] and the addition of the substrates in toluene as reported by Rodríguez *et al*.[18] Both methods were shown to be unsuccessful for our system (Table 4.2, entries 2-3). Subsequently, surfactant was added to the system, since this was reported to increase

catalyst activity by various groups including Mase and coworkers[19] and Cheng and coworkers.[20] However, for our system, both the activity of the catalyst and reproducibility of the system became worse upon addition of surfactant (Table 4.2, entry 4).

Table 4.2: Screening of different reaction conditions to check the reproducibility.

Entry	BTA	$c_{L\text{-pro}}$ (%)	Stack funct.* (%)	Sample treatment	Conversion† (%)	de_{anti}† (%)	ee_{anti}‡ (%)
1	**2**	1	50	Benchmark[a]	69±21	96	98
2	**2**	1	50	Temp. Treat.[b]	18±7	n.d.	n.d.
3	**2**	1	50	Toluene layer[c]	0	-	-
4	**2**	1	50	Surfactant[d]	25±26	74	57
5	**2**	1	50	Plate shaker[e]	>99	30	1
6	**2**	1	50	Vortex mixer[f]	76±9	93	98

* Percentage of **2** mixed with **3**. † Determined by ^{1}H NMR. ‡ Determined by chiral HPLC. [a] Results following the general procedure. [b] The sample was heated to 80 °C, stirred at this temperature for 10 minutes, and slowly cooled down to room temperature (20 °C h^{-1}) before equilibration. [c] The reagents were added dissolved in 125 µL of toluene. [d] 0.67 µM (10 mol% compared to the total BTA concentration in the sample) Triton-X 100 was added to the sonicated sample. [e] 10 glass beads were added to the vial and the sample was fixed on a plate shaker and shaken at 400 rpm during the reaction. [f] The samples were put on a vortex mixer during the reaction. Conditions: stack composition: 50% **2**, 50% **3**; reaction volume: 0.5 ml; aldehyde concentration: 50 mM; substrate ratio (aldehyde:ketone): 1:10; room temperature; reaction time: 24 h.

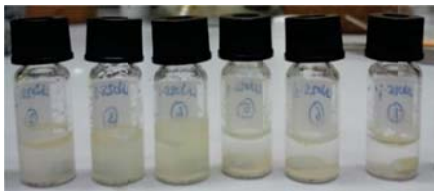

Figure 4.9: Various catalysis samples after 24h reaction time showing the inhomogeneous nature of the samples.

Since the catalysis samples, where a reaction with non-water-soluble substrates is performed in water, are very inhomogeneous (Figure 4.9), we envision the stirring to have an influence on the catalytic activity. Therefore, we designed an alternative setup allowing to keep the substrate better dispersed. In this method, the sample is not stirred with a magnetic stir bar, but several glass beads are added to the vial. Subsequently the vials are fixed to a plate shaker and are shaken at 400 rpm during catalysis (Figure 4.10 A). This method yielded full conversion (Table 4.2, entry 5), but a significantly worse selectivity. In further experiments, samples containing only glass beads and no catalyst showed full conversion and poor selectivity as well. Apparently, the glass beads catalyze the reaction in an unspecific way, something that has not been reported before.

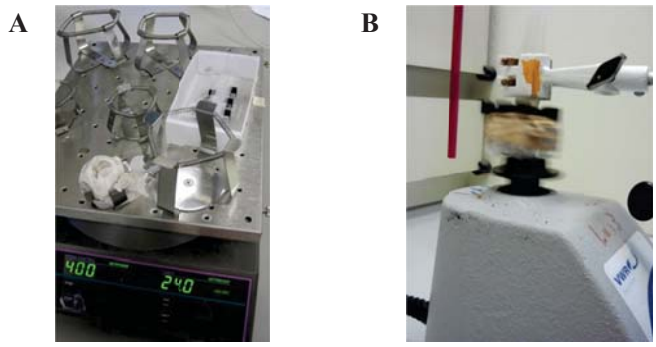

Figure 4.10: Performing the reaction on (A) a plate shaker and (B) a vortex mixer.

Finally, we tried mixing the sample on the vortex mixer during the reaction (Figure 4.10 B). This method yielded both better conversions and reproducibility of the system (Table 4.2, entry 6) compared to the other setups (Table 4.2, entries 1-5). Therefore, mixing by vortex was used for all the remaining experiments.

4.3.2. Excellent reproducible catalytic activity of **2**

The activity, selectivity and reproducibility found in the initial catalysis experiments upon mixing by vortex were promising. Analysis of six additional samples confirmed these results, since a reproducible conversion of 92 ± 8% and excellent selectivities (*de* = 92 ± 3% and *ee* = 97 ± 1%) were obtained (Table 4.3, entry 1).

Table 4.3: 2 as catalyst for aldol reactions.

Entry	BTA	$c_{L\text{-pro}}$ (%)	Stack funct.* (%)	Conversion† (%)	de_{anti}† (%)	ee_{anti}‡ (%)
1	**2**	1	50	92±8	92	97
2	**2**	0.2	50	98±4	74	82
3	**2**	0.1	50	37±5	59	50

* Percentage of **2** mixed with **3**. † Determined by ^{1}H NMR. ‡ Determined by chiral HPLC. Conditions: reaction volume: 0.5 ml; aldehyde concentration: 50 mM; substrate ratio (aldehyde:ketone): 1:10; room temperature; reaction time: 24 h.

Since **2** was found to show excellent activity and selectivity at a catalyst loading of 1 mol% (Table 4.3, entry 1), the catalyst loading was decreased in order to find the minimum catalyst loading that is necessary to obtain an active system. Our catalyst was found to be active at an extremely low loading of 0.2 mol% *L*-proline, where still excellent activity was observed (conversion = 98%, Table 4.3, entry 2). To the best of our knowledge, catalyst loadings of 0.2 mol% are among the lowest reported in literature.[16,21]

If we decrease the catalyst concentration even further to 0.1%, the catalytic activity strongly decreases as only 37% conversion is obtained after 52 hours (Table 4.3, entry 3). Furthermore, the

selectivity was found to decrease upon decreasing the catalyst loading below 1 mol%. (Table 4.3, entries 2-3). The phenomenon was reported in literature before.[21]

4.4. BTAs 1 and 2 compared

We want to compare the catalytic activity and selectivity of **1** and **2** in order to evaluate the influence of the differences in molecular on the catalytic behavior. Accordingly, we repeated the initial experiments performed for **1**, using the improved setup. Since BTA **1** was shown to be active at 3 mol% whereas **2** was shown to be active at 1 mol%, we studied both systems at both catalyst loadings to be able to make a reliable comparison.

Table 4.4: Comparison of the catalytic activity of 1 and 2.

Entry	BTA	$c_{L\text{-pro}}$ (%)	Stack funct.* (%)	Conversion† (%)	de_{anti}† (%)	ee_{anti}‡ (%)
1	**1**	3	100	98±1	63	63
2	**1**	3	50	>99	64	65
3	**1**	1	100	22±2	59	59
4	**1**	1	50	20±2	59	60
5	**2**	3	100	>99	87	95
6	**2**	3	50	>99	89	97
7	**2**	1	100	>99	85	94
8	**2**	1	50	92±2	91	96
9	**3**	1[a]	-	0	-	-

* Percentage of functionalized BTAs mixed with **3**. † Determined by ^{1}H NMR. ‡ Determined by chiral HPLC. [a] *L*-proline was added separately. Conditions: reaction volume: 0.5 ml; aldehyde concentration: 50 mM; substrate ratio (aldehyde:ketone): 1:10; room temperature; reaction time: 24 h.

Using mixing by vortex, **1** showed quantitative conversions and moderate selecivities (de ≈ 64% and ee ≈ 64%) at a catalyst loading of 3% (Table 4.4, entries 1-2). Decreasing the catalyst loading to 1 mol% resulted in a slight decrease in selectivity but a dramatically drop in conversion to ~ 20%. Catalysis with **2** shows yields well above 90% at both a catalyst concentration of 3% and 1% (Table 4.4, entries 5-8). Furthermore, comparable diastereoselectivities above 85% and excellent enantioselectivities around 95% are found for all the experiments. For both **1** and **2**, no significant difference between the samples with exclusively functionalized BTAs and functionalized BTAs mixed with **3** is observed (Table 4.4, entries 1 and 3 versus 2 and 4 and entries 5 and 7 versus 6 and 8). It is plausible that the activity of the *L*-proline in these aggregates remains unaffected since the

local *L*-proline concentration in 50% functionalized stacks is relatively high as still a lot of moieties are present in close proximity.

The importance of covalent attachment of the *L*-proline to the BTAs becomes clear from Table 4.4, entry 9. Upon mixing of **3** with unmodified *L*-proline, no conversion was obtained after 24 hours. This result is not surprising, since the hydrophobic substrates like to be in the hydrophobic interior of the BTAs, whereas the highly water soluble *L*-proline is most likely found in the aqueous phase. This difference in hydrophobicity very likely leads to segregation of the catalyst and the substrate, thereby shutting off the catalysis.

4.4.1. Investigate the recyclability of the catalyst

After the extraction of the aldol products, all BTAs were retained in the aqueous layer, giving rise to the possibility to recycle the catalyst solution. The recycling was done by purging the used aqueous catalyst solution with argon for 10 minutes to remove all diethyl ether remaining from the extractions. Subsequently, new substrates were added and the reaction was performed under the same conditions. Excellent recyclability of the catalyst solutions was found, as both similar conversions and selectivities were obtained for **1** and **2** in the second run (Table 4.5, entries 2 and 4) compared to the fresh catalyst solutions (Table 4.5, entry 1 and 3). Whereas in literature, usually decreased yields and selectivities are reported for reused catalyst solutions,[18] our system allows for complete recovery of the catalytic activity and selectivity by simply bubbling argon through the used solution.

Table 4.5: Investigate recyclability of the system.

Entry	BTA	$C_{L\text{-pro}}$ (%)	Stack funct.* (%)	Conversion† (%)	de_{anti}† (%)	ee_{anti}‡ (%)
1	**1**	3	50	>99	64	65
2[a]	**1**	3	50	>99	71	68
3	**2**	1	50	92	91	96
4[a]	**2**	1	50	96	93	95

[a] Recycled catalyst solution. * Percentage of functionalized BTA mixed with **3**. † Determined by ^{1}H NMR. ‡ Determined by chiral HPLC. Conditions: 50% functionalized BTA, 50% **3**; reaction volume: 0.5 ml; aldehyde concentration: 50 mM; substrate ratio (aldehyde:ketone): 1:10; room temperature; reaction time: 24 h.

4.5. Discussion and conclusion

The catalytic activity of **1** and **2** was studied intensively with the model aldol reaction between 4-nitrobenzaldehyde and cyclohexanone. Initially, **1** was found to be moderately active at a proline concentration of 3%. However, upon optimization of the mixing of the sample, quantitative

conversion is obtained at a catalyst loading of 3% while the reasonable diastereomeric- and enantiomeric excesses around 60% are maintained (Table 4.6, entry 1).

BTA **2** was shown to be a very active catalyst; quantitative conversion is obtained at catalyst loadings as low as 1 mol% (Table 4.6, entry 2). Furthermore, a diastereomeric excess of 96% and an enantiomeric excess of 97% were obtained in individual runs at the same catalyst concentration of 1 mol%. The low error on values averaged over six samples depicts the high reproducibility of both the conversion as well as the excellent selectivity (Table 4.6, entry 3).

For all tested conditions, the selectivities of **2** are significantly better than of **1**, which is a clear indication that the proline moieties are better shielded from the aqueous environment in the new system. Comparison of the catalytic performance of **2** to selected literature examples (Table 4.6, entries 5-8) unambiguously shows both the excellent activity and selectivity of our system. Furthermore, the catalyst is active at lower concentrations than usually described in literature (Table 4.6, entry 4),[16,22] although selectivities slightly decrease at really low catalyst loadings.

Table 4.6: *L*-proline catalyzed aldol reactions under various conditions.

Entry	BTA	Aldehyde conc. [x10^{-3} M]	Stack funct.* (%)	$c_{L\text{-pro}}$ (%)	Conversion† (%)	de_{anti}† (%)	ee_{anti}‡ (%)
1	**1**	50	50	3	>99	64	65
2	**2**	50	100	1	>99	85	94
3	**2**	50	50	1	92±8[a]	92±3[a]	97±1[a]
4	**2**	50	50	0.2	98	74	82
5[a]	-	50	-	5	56	91	98
6[b]	-	50	-	1	>99	90	99
7[c]	-	400	-	10	93	86	96
8[d]	-	125	-	1	96	98	93

* Percentage of functionalized BTA mixed with **3**. † Determined by ^{1}H NMR. ‡ Determined by chiral HPLC. [a] The average and standard deviation is calculated using six experiments. Conditions: reaction volume: 0.5 ml; aldehyde concentration: 50 mM; substrate ratio (aldehyde:ketone): 1:10; room temperature; reaction time: 24 h. [a] Benchmark reaction Huerta *et al.*[6] [b] Benchmark reaction graduation work Van Genabeek.[7] [c] Benchmark reaction Lipschutz *et al.*[14] [d] Benchmark conditions O'Reilly *et al.*[15]

In order to obtain good and reliable catalyst results, 170 catalysis experiments were necessary. Especially in the beginning, the lack of reproducibility was a major issue as roughly one quarter of the experiments did not follow the expected trend. We spent a lot of time to investigate the influence of various variables on the system and by optimization of the experimental procedure, we significantly increased the reproducibility of our experiments and got excellent results. However, the

reproducibility of this system at the lower limit of 0.2 mol% catalyst loading of **2** has still to be improved.

We showed a slight trend of increasing conversion towards higher stack functionalization for **1**. However, we have to be careful with the interpretation of this trend, because the high total BTA concentrations in some samples resulted in gel formation, and stirring of the samples was found to be not optimal. Further research is necessary to solve these issues and to determine the dependence of activity and selectivity of **2** on the local *L*-proline concentration.

4.6. Experimental section

4.6.1. Materials

All reagents were purchased from Aldrich, Acros Organics or Fluka and used as received, unless otherwise specified. HPLC grade solvents were purchased from Scarlab, Biosolve and/or Carlo Erba and use without further purification. All other solvents were purchased from Biosolve.

4.6.2. Methods

^{1}H-NMR spectra were recorded on a Varian Mercury Vx 400 MHz and/or a Varian 400MR 400 MHz (400 MHz for 1H-NMR). Proton chemical shifts are reported in ppm (δ) downfield from trimethylsilane (TMS) using the resonance frequency of the deuterated solvent as the internal standard.

High performance liquid chromatography (HPLC) analyses were carried out on a Shimadzu SCL-10Avp with UV-diode array and equipped with a Chiralpack-IA-3 column (100 x 2.1 mm, 3 μm) from Daicel.

General procedure for the catalysis experiments

A 15 mM stock solution of the catalyst 1 and 2 was prepared in methanol. The appropriate amount of stock solution was transferred to a 1.5 ml vial and the solvent was removed under a stream of argon at room temperature and subsequently in the vacuum oven at 40°C. Water (0.5 ml) was added and the mixture was sonicated for 2 minutes using either a Branson 2510 2510E-DTH sonicator or a VWR Ultrasonic cleaner USC 300T. Equilibration overnight yielded clear solutions.

A mixture of aldehyde (0.025 mmol, 1eq) and ketone (0.250 mmol, 10 eq) was added and the mixture was mixed vigorously for 24 hours at room temperature (unless stated otherwise). The aldol product were extracted with diethyl ether (3x 1 ml) and dried in air. The crude products were analyzed by ^{1}H NMR (400 MHz. $CDCl_3$) (for the determination of the conversion and diastereomeric excess) and chiral HPLC (for the determination of the enantiomeric excess).

Screening of different reaction conditions

Temperature treatment: The temperature treatment was done by heating the sample to 80 °C, stirring at this temperature for 10 minutes, and slowly cooling down to room temperature (20 °C h^{-1}).

Toluene layer: Before addition of the reagents, they were dissolved in 125 μL of toluene. The solution was subsequently added on top of the equilibrated sample.

Surfactant: 0.67 μM (10 mol% compared to the total BTA concentration in the sample) Triton-X 100 was added to the sonicated sample.

Vortex mixer: No magnetic stirring bar was added to the sample, but samples were put on a vortex mixer during the reaction time.

Plate shaker: 10 glass beads were added to the vial and the sample was fixed on a plate shaker and shaken at 400 rpm during the reaction time.

Low-loading experiments

For samples containing 0.2 mol% and 0.1 mol% **2**, samples containing 1 mol% **2** were prepared as described above and diluted after equilibration to give the correct catalyst concentration. 0.5 ml of these diluted samples was transferred to a new vial and equilibrated again prior to use.

4.7. References

(1) Zotova, N.; Franzke, A.; Armstrong, A.; Blackmond, D. G. *J. Am. Chem. Soc.* **2007**, *129*, 15100–15101.
(2) Samanta, S.; Liu, J.; Dodda, R.; Zhao, C.-G. *Org. Lett.* **2005**, *7*, 5321–5323.
(3) Albertazzi, L.; Zwaag, D. van der; Leenders, C. M. A.; Fitzner, R.; Hofstad, R. W. van der; Meijer, E. W. *Science* **2014**, *344*, 491–495.
(4) Frissen, M. *Graduation report*; University of Technology Eindhoven, 2014.
(5) Gosens, R. *Graduation report*; University of Technology Eindhoven, 2014.
(6) Huerta, E.; van Genabeek, B.; Stals, P. J. M.; Meijer, E. W.; Palmans, A. R. A. *Macromol. Rapid Commun.* **2014**, *35*, 1320–1325.
(7) Genabeek, van, B. Designing hydrogen bonding based supramolecular systems for efficient organocatalysis in water.
(8) Huerta, E.; Genabeek, van, B.; Lamers, B. A. G.; Koenigs, M. M. E.; Meijer, E. W.; Palmans, A. R. A. Submitted.
(9) Mlynarski, J.; Baś, S. *Chem. Soc. Rev.* **2013**, *43*, 577–587.
(10) Bahmanyar, S.; Houk, K. N.; Martin, H. J.; List, B. *J. Am. Chem. Soc.* **2003**, *125*, 2475–2479.
(11) Sakthivel, K.; Notz, W.; Bui, T.; Barbas, C. F. *J. Am. Chem. Soc.* **2001**, *123*, 5260–5267.
(12) Wu, Y.; Zhang, Y.; Yu, M.; Zhao, G.; Wang, S. *Org. Lett.* **2006**, *8*, 4417–4420.
(13) Trost, B. M.; Brindle, C. S. *Chem. Soc. Rev.* **2010**, *39*, 1600–1632.
(14) Lipshutz, B. H.; Ghorai, S. *Org. Lett.* **2012**, *14*, 422–425.
(15) Lu, A.; Cotanda, P.; Patterson, J. P.; Longbottom, D. A.; O'Reilly, R. K. *Chem. Commun.* **2012**, *48*, 9699–9701.
(16) Giacalone, F.; Gruttadauria, M.; Agrigento, P.; Noto, R. *Chem. Soc. Rev.* **2012**, *41*, 2406–2447.
(17) Escuder, B.; Rodríguez-Llansola, F.; Miravet, J. F. *New J. Chem.* **2010**, *34*, 1044–1054.
(18) Rodríguez-Llansola, F.; Miravet, J. F.; Escuder, B. *Chem. Commun.* **2009**, 7303–7305.
(19) Mase, N.; Noshiro, N.; Mokuya, A.; Takabe, K. *Adv. Synth. Catal.* **2009**, *351*, 2791–2796.
(20) Peng, Y.-Y.; Ding, Q.-P.; Li, Z.; Wang, P. G.; Cheng, J.-P. *Tetrahedron Lett.* **2003**, *44*, 3871–3875.
(21) Giacalone, F.; Gruttadauria, M.; Agrigento, P.; Lo Meo, P.; Noto, R. *Eur. J. Org. Chem.* **2010**, *2010*, 5696–5704.
(22) Raj, M.; Singh, V. K. *Chem. Commun.* **2009**, 6687–6703.

Conclusion and outlook

In this project, we aimed to use benzene-1,3,5-tricarboxamides (BTAs) as scaffold to construct an enzyme mimic. Two *L*-proline functionalized water soluble BTAs were designed. Their different molecular designs, **1** bearing three proline moieties at the periphery and **2** containing one proline moiety in the hydrophobic interior, were shown to result in different behavior. Both compounds were obtained in high purity *via* a multistep synthesis.

The self-assembly behavior was studied in detail using various techniques including UV-Vis spectroscopy, circulair dichorism (CD) spectroscopy, dynamic light scattering (DLS), small-angle X-ray scattering (SAXS), and cryogenic transmission electron microscopy (cryo-TEM). UV-Vis spectroscopy suggested self-assembly of **2** in dilute aqueous solutions into similar aggregates as previously observed for non-functionalized BTAs. Furthermore, the SAXS data showed the formation of cylinders with a high aspect ratio and ultimately, one-dimensional stacks of **2** could be visualized using cryo-TEM. The UV-Vis absorption curve of **1** was indicative for a different packing, which was confirmed by SAXS, where data characteristic for sphere-like objects with an aspect ratio close to unity were obtained. It is hypothesized that **1** self-assembles into small stacks that do not grow beyond a certain size due to the electrostatic repulsion between charged *L*-proline moieties whereas **2** was shown to self-assemble into one-dimensional stacks.

The catalytic activity of **1** and **2** was studied intensively with the model aldol reaction between 4-nitrobenzaldehyde and cyclohexanone. After optimization of the reaction conditions, **1** showed quantitative conversions, with a diastereoselectivity and enantioselectivity of 64% and 65%, respectively, at a catalyst loading of 3 mol%. BTA **2** was shown to be even more active: quantitative conversion, a diastereomeric excess of 96% and an enantiomeric excess of 97% were obtained in individual runs while the averaged values over six samples depict the high reproducibility of the experiments (conversion = 92 ± 8%, *de* = 92 ± 3%, and *ee* = 97 ± 1%). Furthermore, full conversion and slightly decreased selectivity (*de* = 74%, *ee* = 82%) were obtained at extreme low catalyst loadings of only 0.2 mol% after 24 h reaction time. For all tested conditions, the activity and selectivity of **2** is significantly better compared to **1**, supporting our hypothesis that the *L*-proline is better incorporated into the hydrophobic interior of the supramolecular aggregates formed by **2**.

It was hypothesized that *L*-proline shows better catalytic properties if multiple *L*-proline moieties are present in close proximity. The design of our system allows to test this hypothesis, because the local *L*-proline density in the stacks can be lowered by addition of unfunctionalized BTAs to a system containing **1** or **2**. Dilution of the local *L*-proline concentration of **1** showed a slight trend of increasing conversion towards higher local *L*-proline density. However, further research is necessary to show validity of this trend, because the conditions for catalysis were found to be not optimal. The

dependence of activity and selectivity of **2** on the local *L*-proline concentration has to be determined in further research.

It would be very interesting to optimize the current system in further research, since some questions remain unanswered. For example, we do not know yet whether **1** and **2** coaggregate with non-functionalized BTAs, whereas coaggregation is a prerequisite to achieve dilution of the local *L*-proline concentration. Furthermore, more research regarding activity and selectivity of **2** on the local *L*-proline concentration in the stack is desirable to be able to really construct the envisioned enzyme mimic. Finally, it would be advantageous to gain more understanding of the catalytic system, to further increase the reproducibility of the experiments.

Ultimately, we would like to design a catalytic supramolecular system that is only active upon the introduction of a trigger. Introduction of this trigger causes clustering of the functionalized BTAs, resulting in a high local concentration of *L*-proline moieties. Since *L*-proline is hypothesized to have a higher activity if multiple catalytic moieties are present in close proximity, this will increase the catalytic efficiency of the system. The development of such a stimulus-controlled system would be a great step towards catalytic systems showing similar signal transduction as observed in natural systems.

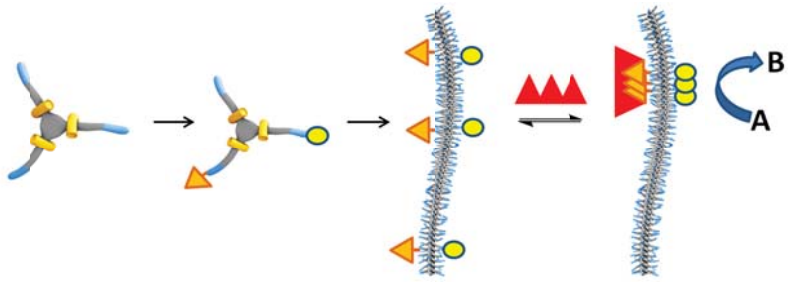

Figure 1: Schematic representation of introduction of functionalized BTAs into a supramolecular stacks and clustering upon introduction of a trigger, thereby enabling a chemical reaction.

In order to achieve clustering of the functionalized BTAs in the supramolecular stacks, we envision clustering of the functionalized receptor BTAs with a multivalent binder that is able to recruit multiple functionalized BTAs. Various of these receptor-binder systems have been explored in literature as well as in our group,[1,2] but their applicability to our system has to be studied in further research.

Finally, it would be interesting to explore the substrate scope of the current system and investigate catalysis with different aldehydes and ketones. Moreover, the catalytic activity of *L*-proline towards various other reactions can be studied. Even further exploration of the possibilities of catalytic BTAs can be done by functionalization of the BTAs with a different (organocatalytic) moiety. These BTAs may be used to catalyze a large variety of reactions in water. A combination of different functionalized BTAs can even be used to perform cascade reactions in an efficient way.

4.1. References

(1) Albertazzi, L.; Martinez-Veracoechea, F. J.; Leenders, C. M. A.; Voets, I. K.; Frenkel, D.; Meijer, E. W. *Proc. Natl. Acad. Sci.* **2013**, *110*, 12203–12208.
(2) Bérubé, M.; Dowlut, M.; Hall, D. G. *J. Org. Chem.* **2008**, *73*, 6471–6479.

Acknowledgements

Achter mij liggen 11 maanden afstudeeronderzoek waarin ik met veel plezier allerlei nieuwe kennis en vaardigheden heb opgedaan. Het tastbare bewijs daarvoor ligt nu voor je, mijn afstudeerverslag. Dit onderzoek was alleen mogelijk dankzij de bijna 300 NMR metingen, talloze TLC's, uren UV-Vis metingen, maar vooral dankzij goede begeleiding en veel advies op verschillende vlakken.

Allereerst wil ik graag Bert Meijer bedanken voor de mogelijkheid om binnen deze vakgroep mijn afstudeer project uit te voeren. Je had een nieuw en uitdagend project voor mij op het oog, dat ik dan ook met veel plezier heb uitgevoerd. Je betrokkenheid, enthousiasme en tips hebben niet alleen mijn onderzoek heel erg vooruit geholpen, maar mij ook als persoon gevormd. De motiverende sfeer die je creëert in deze groep zorg voor een hele prettige werkomgeving.

Janus en Matt, bedankt voor de dagelijkse begeleiding. The advantage of having two supervisors is that you get in touch with different approaches to the same question. Moreover, when I had questions, there was usually one of you around. The challenge, however, is to get everyone on the same page. Although this failed sometimes, I think we did a really good job. Janus, bedankt voor het beantwoorden van al mijn vragen gedurende de afgelopen maanden. Je (soms harde) kritiek, heeft mij geleerd altijd kritisch te blijven ten opzichte van mijn eigen werk. Matt, thank you for all the creative solutions to all the problems (or should I call it challenges?) I encountered during the past months. Furthermore, I learned a lot about research in general and scientific English.

Anja Palmans, bedankt voor het mee denken over mijn project. Jou op- en aanmerkingen in verschillende stadia van het project alsmede je passie voor katalyse hebben ervoor gezorgd dat ik dit project tot een zo goed einde heb kunnen brengen.

Hans Heuts wil ik graag bedanken voor het plaatsnemen in mijn afstudeercommissie.

Ilja Voets, bedankt voor het meten en uitwerken van de SAXS data van mijn verbindingen. Gijs ter Huurne, ik waardeer het heel erg dat je niet alleen de DLS metingen voor mij hebt ingezet, maar we ook de resultaten samen hebben geïnterpreteerd. René Lafleur, heel erg bedankt voor het doen van de cryo-TEM metingen. Ik ben heel blij met de resultaten, immers, zien is geloven.

I would like to thank Ralf Bovee, Joost van Dongen and Xianwen Lou for their assistance with the analysis of my compounds.

Henk, dank voor het draaiende houden van de printer en zo veel meer. Hans Damen, dank voor het bestellen van de benodigde chemicaliën

Furthermore, I want to thank everyone in the water soluble BTA lunch meetings for all help en suggestions regarding my research. Furthermore, I would like to thank all the members of lab 3, for all their help during the lab work.

Ook wil ik graag mijn (voormalige) kantoorgenootjes bedanken, daar zij medeverantwoordelijk waren voor de goede sfeer: Dominique, Robin, Simone, Erik, Ronald, Perry en Roy. Vooral de gesprekken over voetbal vond ik zeer aangenaam, omdat ik elke keer weer het gevoel kreeg dat ik toch één probleem minder heb in mijn leven <

Bas, bedankt voor de ontspanning op de mountainbike alsmede inhoudelijke hulp onder het genot van een ijsje, kopje koffie/thee, blikje radler 0.0% of kasteelbiertje.

Al mijn vrienden binnen en buiten de faculteit wil ik graag bedanken voor de gezellige tijd die ik gehad heb.

Mama, Hugo, Viola, Myrte, bedankt voor de gezelligheid en ontspanning thuisthuis. Papa, Barbara, Johanna und Katharina, ihr habt nicht so viel mitbekommen von meinen genauen Tätigkeiten, aber trotzdem wahrt ihr immer für mich da (oder auch nicht, wenn gerade Chorprobe war, genau dann wenn ich gerade ans telefonieren gedacht habe). Tot slot, Thijs bedankt voor de onvoorwaardelijke steun de laatste tijd. Na samen gestudeerd, bestuurd, en afgestudeerd te hebben is het nu tijd voor de volgende stap.